JACS
JOURNAL OF THE AMERICAN CHEMICAL SOCIETY
Article
pubs.acs.org/JACS

Molecular and Electronic Structure of Dinuclear Uranium Bis-μ-Oxo Complexes with Diamond Core Structural Motifs

Anna-Corina Schmidt,[†] Frank W. Heinemann,[†] Wayne W. Lukens, Jr.,*[,‡] and Karsten Meyer*[,†]

[†]Inorganic Chemistry, Department of Chemistry and Pharmacy, Friedrich-Alexander University of Erlangen-Nürnberg (FAU), Egerlandstr. 1, 91058 Erlangen, Germany

[‡]Lawrence Berkeley National Laboratory, MS 70A-1150, Berkeley, California 94720, United States

Supporting Information

ABSTRACT: In a multiple-bond metathesis reaction, the triazacyclononane (tacn)-anchored methyl- and neopentyl (nP)-substituted tris(aryloxide) U^{III} complex $[((^{nP,Me}ArO)_3tacn)U^{III}]$ (**1**) reacts with mesityl azide and CO_2 to form mesityl isocyanate and the dinuclear bis(μ-oxo)-bridged U^V/U^V complex $[\{((^{nP,Me}ArO)_3tacn)U^V\}_2(\mu\text{-}O)_2]$ (**3**). This reaction proceeds via the mononuclear U^V imido intermediate $[((^{nP,Me}ArO)_3tacn)U^V(NMes)]$ (**2**), which has been synthesized and fully characterized independently. The dimeric U^V oxo species shows rich redox behavior: complex **3** can be reduced by one and two electrons, respectively, yielding the mixed-valent U^{IV}/U^V bis(μ-oxo) complex $[K(crypt)][\{((^{nP,Me}ArO)_3tacn)U^{IV/V}\}_2(\mu\text{-}O)_2]$ (**7**) and the U^{IV}/U^{IV} bis(μ-oxo) complex $K_2[\{((^{nP,Me}ArO)_3tacn)U^{IV}\}_2(\mu\text{-}O)_2]$ (**6**). In addition, complex **3** can be oxidized to provide the mononuclear uranium(VI) oxo complexes $[((^{nP,Me}ArO)_3tacn)U^{VI}(O)_{eq}(OTf)_{ax}]$ (**8**) and $[((^{nP,Me}ArO)_3tacn)U^{VI}(O)_{eq}]SbF_6$ (**9**). The unique series of bis(μ-oxo) complexes also shows notable magnetic behavior, which was investigated in detail by UV/vis/NIR and EPR spectroscopy as well as SQUID magnetization studies. In order to understand possible magnetic exchange phenomena, the mononuclear terminal oxo complexes $[((^{nP,Me}ArO)_3tacn)U^V(O)(O\text{-pyridine})]$ (**4**) and $[((^{nP,Me}ArO)_3tacn)U^V(O)(O\text{-}NMe_3)]$ (**5**) were synthesized and fully characterized. The magnetic study revealed an unusually strong antiferromagnetic exchange coupling between the two U^V ions in **3**. Examination of the ^{18}O-labeled bis(μ-oxo)-bridged dinuclear complexes **3**, **6**, and **7** allowed for the first time the unambiguous assignment of the vibrational signature of the $[U(\mu\text{-}O)_2U]$ diamond core structural motif.

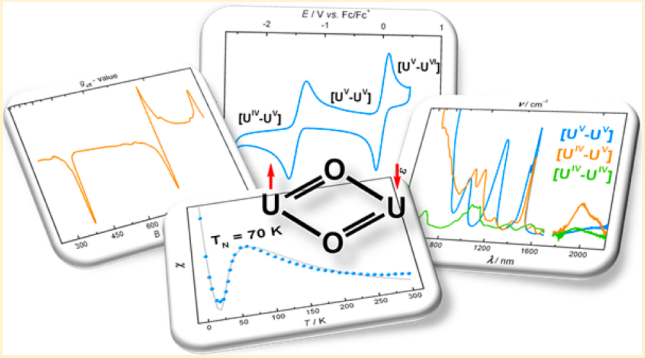

INTRODUCTION

Although the uranyl unit, $[O{=}U{=}O]^{2+}$, is ubiquitous in uranium chemistry,[1] few terminal monooxo uranium complexes – and even fewer with a dinuclear [U=O] motif – have been reported in the literature.[2] Uranium oxo complexes with the same coordination environment but different oxidation states are particularly rare.[3] Therefore, our interests have focused on the role that the metal oxidation state plays in the structure, reactivity, and spectroscopic properties of a series of complexes with nearly identical core structures. From such a homologous structural series, we can draw new insights into the electronic structures and reactivity of uranium oxo complexes, which may improve our fundamental understanding of the role that f orbitals play in uranium–ligand multiple bonding. While bonds in 4f-element complexes have generally been considered to be ionic,[4] the degree of covalency in the M–L bond of 5f complexes, and uranium in particular, remains an important subject of debate.[5] The greater radial extension of the 5f valence orbitals of the early actinides can provide increased overlap with ligand orbitals, thereby enhancing the correlated magnetic behavior between bridged metal centers within a single unit, such as the structurally and electronically interesting diamond core, $M(\mu\text{-}O)_2M$. In the series of complexes presented here, considerably different magnetic behavior is observed depending on the oxidation state. Furthermore, the interplay between strong spin-orbit coupling and a low-symmetry crystal field may result in fascinating but intrinsically difficult to rationalize electronic properties, including magnetic exchange phenomena. Magnetic superexchange, while well-investigated and understood in transition-metal coordination chemistry, is receiving increasing attention in actinide coordination and organometallic chemistry.[6] Antiferromagnetic exchange interactions, for instance, have been observed for most transition-metal and f-element compounds, and Néel temperatures (T_N, defined as the temperature at which the magnetic susceptibility of an antiferromagnetically coupled system reaches its maximum) of up to 1145 K are known for transition-metal oxides or alloys.[7] While transition-metal complexes exhibit Néel temperatures of up to 270 K,[8] only relatively low values have been observed for

Received: May 10, 2014
Published: June 17, 2014

   dx.doi.org/10.1021/ja504528n | J. Am. Chem. Soc. 2014, 136, 11980–11993

Scheme 1. Reaction Scheme for the Synthesis of Complexes 2–9[a]

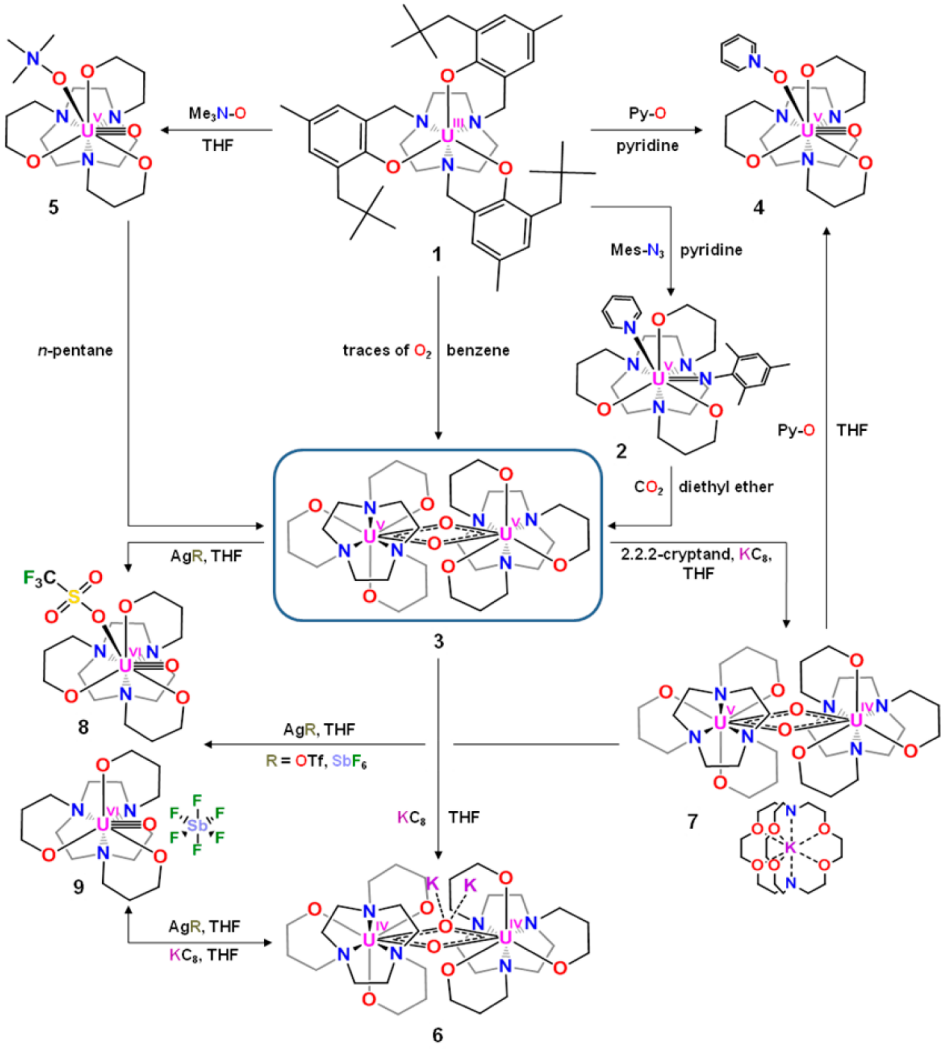

[a]Phenolate rings, including the neopentyl and methyl substituents, have been omitted for clarity.

lanthanide and actinide complexes. This weak coupling is directly related to weak interactions and small covalent contributions to the metal–ligand bonding in f-element complexes. By far the highest value of T_N for a diuranium complex, 110 K, was published by Cummins and co-workers in 2000.[6i,9] In a landmark publication, Rosen, Andersen, and Edelstein reported a dinuclear U^V organoimide that exhibits strong exchange coupling and a T_N of 20 K.[6e] Other U^V complexes exhibit T_N values ranging from 5 to 17 K.[6a–d,f,g]

We now report the synthesis of three dinuclear uranium complexes bridged by two oxo ligands, which results in a diamond-shaped $[U(\mu\text{-}O)_2U]$ structural motif. The principal complex, the dinuclear bis(μ-oxo)-bridged U^V/U^V complex $[\{((^{nP,Me}ArO)_3tacn)U^V\}_2(\mu\text{-}O)_2]$ (tacn = triazacyclononane, nP = neopentyl), possesses a remarkably high Néel temperature of approximately 70 K, suggesting unusually strong exchange interactions within the $[U^V(\mu\text{-}O)_2U^V]$ core. In order to understand the magnetic properties of this compound, mononuclear uranium(V) imido, uranium(V) and uranium(VI) oxo complexes are presented as well for comparison. These new complexes have been characterized by a combination of single-crystal X-ray diffraction, ^{1}H NMR spectroscopy, elemental analysis, mass spectrometry, cyclic voltammetry, UV/vis/NIR electronic absorption spectroscopy, IR/Raman vibrational spectroscopy (including ^{18}O isotope labeling experiments), electron paramagnetic resonance (EPR) spectroscopy, and variable-temperature magnetic susceptibility measurements.

RESULTS AND DISCUSSION

Synthesis. In order to synthesize high-valent oxo and imido complexes of $[((^{nP,Me}ArO)_3tacn)U^{III}]$ (**1**),[10] a solution of **1** in pyridine was treated with mesityl azide. The reaction led to an immediate color change from red to black-brown with concomitant evolution of N_2 gas to yield the U^V imido complex $[((^{nP,Me}ArO)_3tacn)U^V(NMes)]$ (**2a**) as an analytically pure dark-brown powder in a moderate yield of 42% (Scheme 1). The addition of pyridine *N*-oxide (py-O) or trimethylamine *N*-oxide (Me_3N-O) to a solution of **1** also results in a color change to orange-yellow to give the eight-coordinate, terminal U^V oxo complexes $[((^{nP,Me}ArO)_3tacn)U^V(O)(py\text{-}O)]$ (**4**) and $[((^{nP,Me}ArO)_3tacn)U^V(O)(Me_3N\text{-}O)]$ (**5**), respectively (Scheme 1) as analytically pure bright-yellow powders in moderate to good yields (45% for **4** and 68% for **5**). However, the formation of a bis(μ-oxo) complex analogous to $[\{((^{Ad,Me}ArO)_3N)U(py\text{-}O)\}(\mu\text{-}O)_2\{((^{Ad,Me}ArO)_3N)U\}]$, as ob-

dx.doi.org/10.1021/ja504528n | J. Am. Chem. Soc. 2014, 136, 11980–11993

served in a similar reaction with the N-anchored system [{((Ad,MeArO)$_3$N)U^{III}], was not observed.[2g]

Instead, the dinuclear U^V/U^V bis(μ-oxo) complex [{((nP,MeArO)$_3$tacn)U^V}$_2$(μ-O)$_2$] (**3**) was synthesized by forming **2** in situ in diethyl ether and introducing CO_2 under vigorous stirring. After the reaction mixture was cooled to −35 °C, a microcrystalline precipitate formed, and it was filtered off and dried in vacuo to give **3** (Scheme 1) as a dark-purple microcrystalline solid in moderate yield (42%). Complex **3** was also synthesized in low yield via reaction of **1** with SeO_2, trimethylamine *N*-oxide (in *n*-pentane with heat), 2,2,6,6-tetramethylpiperidine *N*-oxyl (TEMPO), and interestingly, low concentrations of neat dioxygen. For the dinuclear complex **3**, electrospray ionization mass spectrometry (ESI-MS) shows a single molecular peak corresponding to the dimeric [**3**]$^+$ complex at m/z = 1902. Positive-ion-mode electron impact (EI+) mass spectrometry shows the molecular peak for the dimeric compound as well. These results indicate that complex **3** exists as a dimer in both the solid state and solution. Reduction of **3** in benzene with excess KC_8 results in a slow color change to green-brown and yields the doubly reduced U^{IV}/U^{IV} complex K$_2$[{((nP,MeArO)$_3$tacn)U$^{IV/IV}$}$_2$(μ-O)$_2$] (**6**) (Scheme 1) as an analytically pure pale-green powder in excellent yield (96%). Using only 1 equiv of KC_8 in the presence of equimolar amounts of 2.2.2-cryptand dissolved in THF results in a fast color change to yellow-brown and formation of the mixed-valent U^{IV}/U^V complex [K(2.2.2-crypt)][{((nP,MeArO)$_3$tacn)U$^{V/IV}$}$_2$(μ-O)$_2$] (**7**) (Scheme 1). By means of this synthetic protocol, **7** was isolated as a yellow-beige powder in good yield (56%). Interestingly, complete conversion to mixed-valent **7** can also be achieved by comproportionation of equimolar amounts of pentavalent **3** and tetravalent **6** in the presence of 1 equiv of 2.2.2-cryptand. It is noteworthy that reduction of the terminal oxo complexes **4** and **5** with KC_8 (in an attempt to prepare mononuclear tetravalent oxo species) did not proceed. In light of the stability of the dinuclear U^{IV}/U^{IV} complex **6** as well as previous[2g,11] isolation of U^{IV} complexes with terminal oxo ligands, this result is all the more remarkable.

Finally, attempts to synthesize the oxidized dinuclear U^V/U^{VI} and U^{VI}/U^{VI} complexes with Ag salts ($AgBAr_{F24}$, $AgBPh_4$, $AgBF_4$, $AgNTf_2$, AgI, $AgNO_2$, AgO, Ag_2O, Ag[Al(OC(CF$_3$)$_3$)$_4$]) and various other oxidizing reagents (I_2, $NOBF_4$, CuSCN, CuCN, $(NH_4)_2Ce(NO_3)_6$, Au_2S, [NMe$_2$(C$_{18}$H$_{37}$)$_2$][Au(C$_3$S$_5$)$_2$], [Fe(Cp)$_2$]PF$_6$, [Co(Cp)$_2$]PF$_6$, NO[Al(OC(CF$_3$)$_3$)$_4$]) incorporating weakly or even noncoordinating anions remained unsuccessful. Instead, the oxidation of dimeric **3** with excess silver triflate or silver hexafluoroantimonate lead to the formation of black, monomeric, terminal U^{VI} oxo complexes, namely, eight-coordinate [((nP,MeArO)$_3$tacn)U^{VI}(O)(CF$_3$SO$_3$)] (**8**) and seven-coordinate [((nP,MeArO)$_3$tacn)U^{VI}(O)][SbF$_6$] (**9**), in good to excellent yields (63% for **8** and 89% for **9**). The reaction of **3** with exactly 1 equiv of AgOTf or $AgSbF_6$ results in conversion of half of the starting material to yield monomeric species **8** or **9**, respectively, whereas the rest remains as the U^V/U^V dimer. To the best of our knowledge, no dinuclear, doubly bridged U^V/U^{VI} or U^{VI}/U^{VI} complexes are known except for those containing the uranyl moiety.[12]

All of the complexes shown in Scheme 1, whose formulas and compound labels are collected in Chart 1, were isolated in moderate to excellent yields and characterized by ^{1}H NMR spectroscopy, single-crystal X-ray diffraction, cyclic voltammetry, UV/vis/NIR absorption spectroscopy, and IR vibrational spectroscopy. The electronic structure and magnetic properties were studied by X-band EPR spectroscopy and superconducting quantum interference device (SQUID) magnetization measurements. The purities of the bulk materials were confirmed by CHN elemental analyses, except for fluoride-containing complexes **8** and **9**, where the possible formation of hazardous, volatile UF_6 precluded elemental analysis. In addition to elemental analysis, the title complexes **3**, **6**, and **7** were characterized by mass spectrometry and vibrational spectroscopy (Raman and IR), including its ^{18}O-labeled isotopomers.

Chart 1. Complex Formulas and Numbers of New Uranium Complexes 2−9 Obtained from the Starting Complex [((nP,MeArO)$_3$tacn)U^{III}] (1)

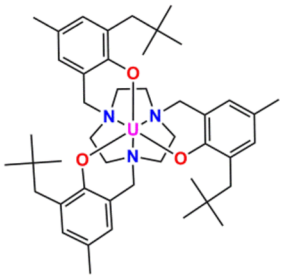

Number	Complex
1	[((nP,MeArO)$_3$tacn)U^{III}]
2	[((nP,MeArO)$_3$tacn)U^V(NMes)(py)]
3	[{((nP,MeArO)$_3$tacn)U^V}$_2$(μ-O)$_2$]
4	[((nP,MeArO)$_3$tacn)U^V(O)(py-NO)]
5	[((nP,MeArO)$_3$tacn)U^V(O)(Me$_3$NO)]
6	K$_2$[{((nP,MeArO)$_3$tacn)U$^{IV/IV}$}$_2$(μ-O)$_2$]
7	[K(2.2.2-crypt)][{((nP,MeArO)$_3$tacn)U$^{V/IV}$}$_2$(μ-O)$_2$]
8	[((nP,MeArO)$_3$tacn)U^{VI}(O)(CF$_3$SO$_3$)]
9	[((nP,MeArO)$_3$tacn)U^{VI}(O)][SbF$_6$]

Structural Characterization. In general, the uranium ion in eight-coordinate complexes **2**−**8** is situated in a distorted trigonal-dodecahedral coordination environment, with a neutral donor ligand occupying the axial position above a square plane formed by the three aryloxides and the oxo/imido ligand; the uranium ion lies slightly below this square plane. The amine nitrogen atoms of the triazacyclononane (tacn) anchor form a trigonal plane opposite the neutral donor ligand (pyridine *N*-oxide, trimethylamine *N*-oxide, pyridine). For complex **9**, the uranium ion is seven-coordinate, with a similar ligand environment as described earlier but with a free axial coordination site. In dinuclear complexes **3**, **6**, and **7**, two trigonal-dodecahedral polyhedra are connected by two bridging oxygen atoms (one axial and one equatorial oxygen; see Figure 1B).

These complexes may also be viewed as *distorted octahedra* with the three amine nitrogen atoms of the tacn ligand occupying a single coordination site trans to the axial neutral

dx.doi.org/10.1021/ja504528n | J. Am. Chem. Soc. 2014, 136, 11980−11993

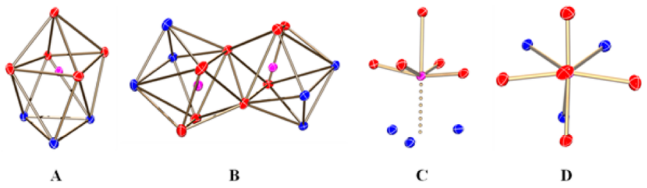

Figure 1. Trigonal-dodecahedral environment for (A) monomeric and (B) dinuclear complexes. (C) Simplified distorted octahedral environment. (D) Top view of (C) along the axial O−U bond, illustrating the C_s symmetry for **3**, **4**, **5**, **6**, **7**, and **8**. Colors: blue, nitrogen; red, oxygen; magenta, uranium.

donor ligand, which is best illustrated in Figure 1C. The description of the coordination as distorted octahedral simplifies the description and fits the explanation of the electronic properties of these complexes (vide infra).

Multiple-bond metathesis of CO_2 with U^V imido complexes of the related adamantyl- and *tert*-butyl-functionalized tris(aryloxide) tacn systems $[(({}^{R,R'}ArO)_3tacn)U^V(NMes)]$ (R = *t*-Bu, Ad; R′ = *t*-Bu, Me) yielded mononuclear U^V oxo complexes.[13] In these complexes, as well as in the imido precursor, the terminal, strongly π-donating oxo/imido ligand is situated on the threefold axis of the C_3-symmetric complex. Clearly, the most prominent structural aspect of the neopentyl-derivatized tacn system is the formation of the high-valent dinuclear bis(μ-oxo)-bridged complex **3** with a diamond core structural motif, $[U^V(\mu\text{-}O)_2U^V]$, along with its one-electron-reduced mixed-valent anion $[U^{IV}(\mu\text{-}O)_2U^V]^-$ (**7**) and doubly reduced anion $[U^{IV}(\mu\text{-}O)_2U^{IV}]^{2-}$ (**6**). In **7**, the complex anion is isolated from the encrypted potassium cation, while in **6**, both potassium ions interact with one of the two bridging oxo ligands. Any attempt to remove the two μ-O-bound K^+ ions in **6** with retention of the diamond core structure remained unsuccessful.[14] Despite these significant structural differences, especially for **6**, the metrics within the diamond cores of **3**, **6**, and **7** are remarkably similar (Figures 2 and 3 and Table 2). In complex **3** and **7**, each bridging oxo ligand occupies an axial site on one uranium center and an equatorial site on the other. The shorter, equatorially bound oxo is situated within the plane of the three aryloxide ligands; thus, forming a square plane with the longer, axial oxo ligand nearly perpendicular to this plane. For complex **6**, however, the bridging oxo ligand that interacts with the potassium ions, occupies the axial position on both uranium ions, while the other bridging oxo ligand occupies an equatorial position.

Complex **3** possesses an inversion center in its diamond core; thus, the two equivalent uranium ions are perfectly in plane with the two bridging oxo ligands. The observed asymmetry of the U−O bond distances within the core is most distinct in $[U^V(\mu\text{-}O)_2U^V]$, with alternating short U−O_{eq} bonds at 2.066(2) Å and longer U−O_{ax} bonds at 2.206(2) Å. The core structure is further characterized by the O−U−O and U−O−U angles, which were determined to be 71.55° and 108.45°, respectively. This leads to a relatively short U···U distance of 3.422(3) Å, which compares well to the U···U separation of 3.3557(5) Å reported by Arnold, Love, and co-workers.[6f]

Remarkably, the core structural motif remains largely unperturbed upon reduction. The O−U−O and U−O−U angles are all very similar at approximately 82° and 108°. While the $[U(\mu\text{-}O)_2U]$ moiety remains nearly planar (deviation from planarity = 2.23° in **6** and 0.9° in **7**), the U···U distances in these complexes show a clear trend with the degree of reduction (Table 2). Accordingly, the shortest U···U distance is found in **3** (3.422(3) Å) and the longest in doubly reduced **6** (3.509(4) Å), while the U···U distance in mixed-valent **7** was determined to be in-between those of **3** and **6** at 3.465(5) Å. As one progresses from **3** to one- and two-electron-reduced **7** and **6**, respectively, the difference between the short and long U−O bonds becomes less pronounced. Consequently, **6** possesses a nearly symmetric core with similar U−O bond distances of 2.166(3) and 2.179(3) Å. The latter observation is particularly surprising since two potassium cations are bound to one of the two bridging oxo ligands of **6**.[14]

We recently reported the synthesis of the bis(μ-oxo)-bridged diuranium species $[\{(({}^{Ad,Me}ArO)_3N)(py\text{-}O)U\}(\mu\text{-}O)_2\{(({}^{Ad,Me}ArO)_3N)U\}]$, which was obtained by treatment of $[(({}^{Ad,\,Me}ArO)_3N)U^{III}]$, the single N-anchored tris(aryloxide) derivative of **1**, with pyridine *N*-oxide. However, a similar treatment of **1** does not produce dimeric **3**. Instead, oxidation of **1** with pyridine *N*-oxide or trimethylamine *N*-oxide yields mononuclear U^V complexes **4** and **5**, $[(({}^{nP,Me}ArO)_3tacn)U^V(O)(L)]$ with L = py-O and Me_3N-O, respectively. As mentioned before, all previously reported pentavalent uranium complexes of the tacn ligand systems with *tert*-butyl and adamantyl substituents in the ortho position, namely, $[(({}^{R,R'}ArO)_3tacn)U^V(L_{ax})]$ (R = R_{ortho} = *t*-Bu, Ad; R′ = R_{para} = *t*-Bu, Me; L_{ax} = O, NTMS, NMes) are seven-coordinate with the strongly π-donating oxo and imido ligands located on the threefold axis of these C_3-symmetric complexes.[15] Only upon oxidation to the hexavalent state do oxo and imido U^{VI} complexes of this ligand system display the *inverse trans influence* (ITI).[2j,16] Consequently, their molecular structures show approximate C_s symmetry with the strongly π-donating ligand in the equatorial plane trans to a mutually enforced, strongly bound aryloxide ligand of the hexadentate chelate. In stark contrast, all monomeric pentavalent uranium complexes of the new neopentyl-derivatized tacn system,

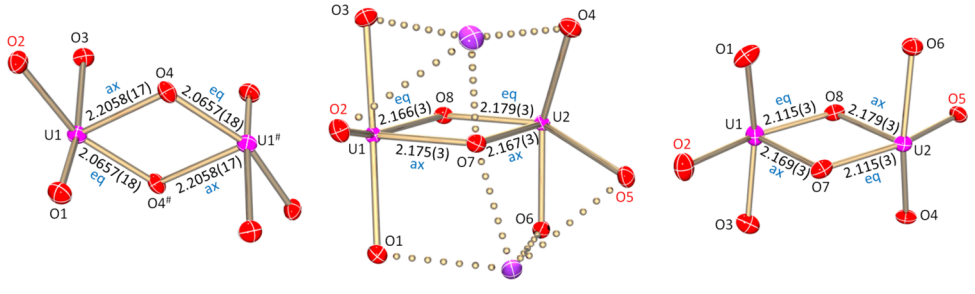

Figure 2. Diamond core structures of the dinuclear complexes **3** (left), **6** (middle), and **7** (right). U−O bond distances in Å are shown. The aryloxide oxo ligands coordinated trans to the equatorial bridging oxo ligands are labeled in red.

dx.doi.org/10.1021/ja504528n | J. Am. Chem. Soc. 2014, 136, 11980−11993

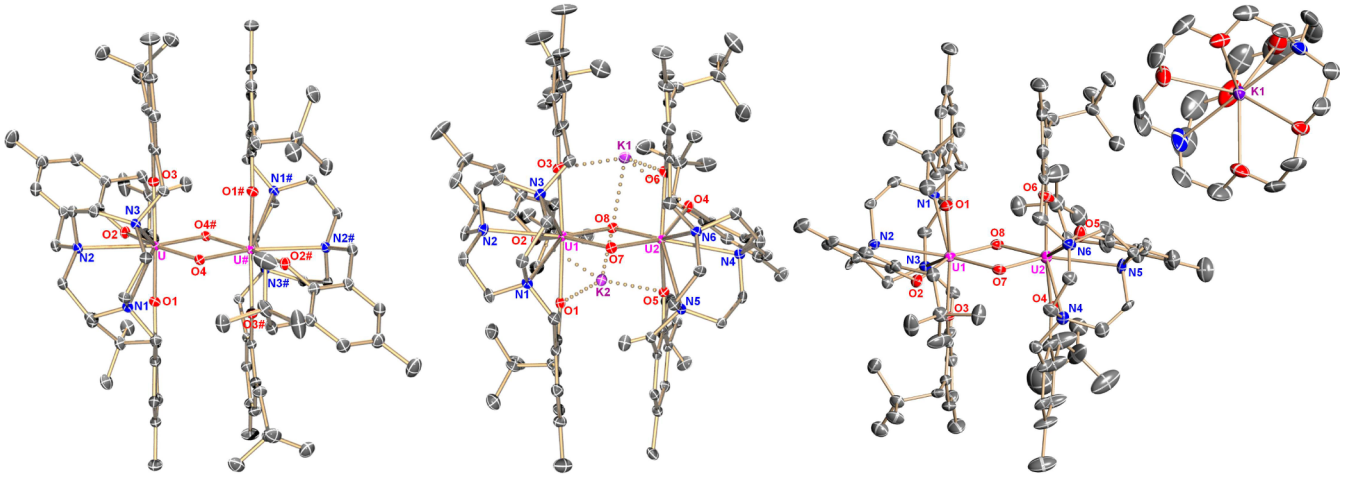

Figure 3. Molecular structures of the dinuclear uranium oxo complexes: (left) U^{V}/U^{V} **3** in crystals of **3**·4C_6H_6; (middle) U^{IV}/U^{IV} **6** in crystals of **6**·6THF; (right) U^{IV}/U^{V} **7** in crystals of **7**·3C_6H_6. H atoms and cocrystallized solvent molecules have been omitted for clarity. Thermal ellipsoids are at 50% probability.

Table 1. Selected Bond Distances (Å) and Angles (deg) for the Mononuclear Complexes 1, 2, 4, 5, 8, and 9

complex	1	2	4[a]		5	8	9[a]	
U–O_{oxo}	–	–	1.856(2)	1.859(2)	1.860(2)	1.794(2)	1.791(6)	1.800(6)
U–$O_{ArO,av}$	2.287	2.215	2.186	2.198	2.204	2.101	2.088	2.101
U–O_{ligand}	2.669(2)	–	2.412(2)	2.407(2)	2.360(2)	2.436(2)	–	–
U–N_{imido}	–	1.979(3)	–	–	–	–	–	–
U–$N_{tacn,av}$	2.517	2.789	2.856	2.861	2.867	2.747	2.613	2.625
U–N_{ligand}	–	2.583(4)	–	–	–	–	–	–
U_{oop}	−0.362	−0.408	−0.420	−0.351	−0.200	−0.388	−0.758	−0.709
O/N_{oop}	–	+0.285	−0.209	−0.063	+0.240	−0.266	−0.504	−0.339
O/N–U–O_{trans}	–	148.80(12)	161.29(8)	160.46(8)	160.87(10)	160.73(8)	149.7(3)	147.8(3)
O_{cis}–U–O_{cis}[b]	–	157.00(10)	157.92(7)	161.86(7)	161.26(8)	158.04(7)	137.9(2)	140.9(2)

[a]There are two independent molecules in the unit cells of **4** and **9**. [b]O_{cis} is the aryloxo arm cis to the terminal oxo/imido ligand

Table 2. Selected Bond Distances (Å) and Angles (deg) for the Dinuclear Complexes 3, 6, and 7

complex	3	6	7
U(1;2)–O_{oxo}	2.0354(12), 2.1815(11)	2.1259(17), 2.1928(16); 2.2012(16), 2.1445(16)	2.115(3), 2.169(3); 2.179(3), 2.115(3)
U(1;2)–$O_{ArO,av}$	2.1827	2.3822; 2.3582	2.247; 2.258
U(1;2)–$N_{tacn,av}$	2.8017	2.805; 2.784	2.811; 2.811
U(1)–U(2)	3.4222(3)	3.5090(4)	3.4653(5)
$U(1;2)_{oop}$	−0.219	−0.224; −0.181	−0.179; −0.138
O/N_{oop}	+0.263	+0.610; +0.636	+0.365; +0.470
π–π/π–$C_{nP,tacn,av}$[a]	3.623 (π–π)	3.730 (π–$C_{nP,tacn}$)	3.758, 3.655 (π–π)
U(1;2)–O–U(2;1)	108.45(5)	108.36(7); 107.99(7)	108.00(13); 107.60(12)
O–U(1;2)–O	71.55(5)	72.05(6); 71.54(6)	72.30(11); 72.09(11)
U–$(O)_2$–U[b]	0.00	2.23	0.90
O/N–U(1;2)–O_{trans}	159.97(5)	148.65(6); 149.54(6)	159.87(11); 157.94(11)
O_{cis}–U(1;2)–O_{cis}[c]	158.38(4)	156.55(6); 152.16(6)	158.77(12); 158.39(11)

[a]Distance of the aromatic ring to the carbon atom from the neopentyl group or the tacn ring, where a π–CH bond interaction is possible. [b]Torsion angle. [c]O_{cis} is the aryloxo arm cis to the terminal oxo/imido ligand

$[((^{nP,Me}ArO)_3tacn)U^{V}(L)]$, have the terminal oxo and imido ligands in the equatorial plane along with the three aryloxide pendant arms of the hexadentate chelate. In the presence of the neutral donor ligands pyridine *N*-oxide, trimethylamine *N*-oxide, or pyridine, the coordination sphere of these complexes is completed by a usually weakly bound donor ligand in the axial position trans to the tacn anchor. Regardless of these drastically different coordination environments, the U–O bond distances are almost the same, with values of 1.856(2) and 1.859(2) Å for the two independent molecules in the structure of **4** and 1.860(2) Å for **5** (Table 1), in comparison with 1.848(4) and 1.848(8) Å for $[((^{R,R'}ArO)_3tacn)U^{V}(O)]$ (R = Ad, *t*-Bu; R′ = *t*-Bu), respectively, and other U^{V} terminal oxo complexes.[2d−f,13]

Attempts to oxidize the dinuclear complexes **3**, **6**, and **7** to obtain the corresponding complexes with $[U^{V}(\mu\text{-}O)_2U^{VI}]$ or $[U^{VI}(\mu\text{-}O)_2U^{VI}]$ core structures led only to the isolation of mononuclear U^{VI} complexes with terminal oxo ligands, namely, $[((^{nP,Me}ArO)_3tacn)U^{VI}(O)_{eq}(CF_3SO_3)_{ax}]$ (**8**) and

dx.doi.org/10.1021/ja504528n | J. Am. Chem. Soc. 2014, 136, 11980−11993

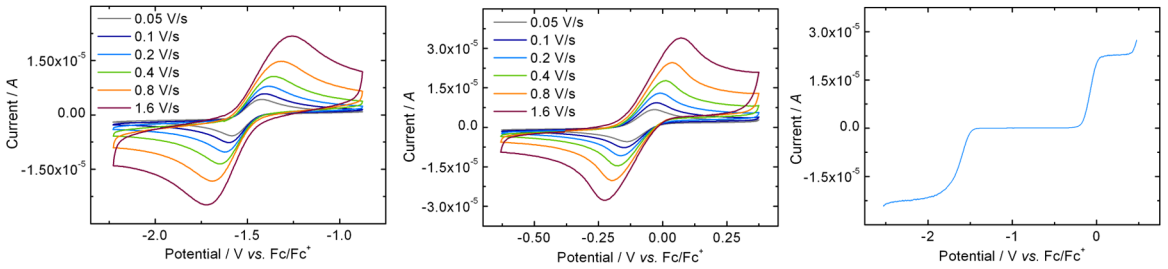

Figure 4. (left) Reversible reduction wave and (middle) reversible oxidation wave of **3** at different scan rates. (right) Linear-sweep measurement in ~0.1 M $[N(n\text{-}Bu)_4][PF_6]$ in THF at room temperature. The scan was collected at 50 mV/s with a step potential of 2 mV.

$[(({}^{nP,Me}ArO)_3tacn)U^{VI}(O)_{eq}][SbF_6]$ (**9**). U^{VI} complexes with a single terminal oxo ligand represent a rare class of complexes with few reported examples.[2h−m] The monomeric U^{VI} terminal oxo complexes **8** and **9** possess coordination environments similar to those of **4** and **5** as well as to those of known complexes of the *tert*-butyl- and adamantyl-derivatized tacn systems (with complex **9** missing the axial ligand).[2j] As in **4** and **5**, the terminal oxo ligand in **8** is in the equatorial position along with the three aryloxides, and the weakly coordinating triflate counterion is bound in axial position trans to the tacn anchor. The very short $U-O_{oxo}$ bond (1.794(2) Å in **8** vs 1.811(2) Å for $[(({}^{t\text{-}Bu,t\text{-}Bu}ArO)_3tacn)U^{VI}(O)(CF_3COO)]$ and 1.836(6) Å for $[(({}^{t\text{-}Bu,t\text{-}Bu}ArO)_3tacn)U^{VI}(O)][SbF_6]$) is due to the ITI and results from the mutually reinforced bonding within the nearly linear $O_{ArO}-U-O_{oxo}$ arrangement (160.73(8)° in **8** vs 159.67(6)° for $[(({}^{t\text{-}Bu,t\text{-}Bu}ArO)_3tacn)U^{VI}(O)(CF_3COO)]$ and ~149° for $[(({}^{t\text{-}Bu,t\text{-}Bu}ArO)_3tacn)U^{VI}(O)][SbF_6]$). Similar short $U-O_{oxo}$ bond distances have been reported for other U^{VI} terminal oxo complexes.[2i,l] For complex **9**, the SbF_6^- counteranion is not coordinated at the axial position, which leaves an open coordination site. Although the $O_{ArO}-U-O_{oxo}$ angle in **9** is more acute at 149.7(3)° and 147.8(3)° because of the missing axial ligand, **9** still shows similarly short $U-O_{oxo}$ bonds (1.791(6) and 1.800(6) Å). The U═NMes bond length of 1.979(3) Å in **2** is similar to those previously reported for U^V imido complexes (1.935 to 2.122 Å).[13,15] The uranium−pyridine bond length of 2.583(4) Å is in the range for other reported U−N bonds with neutral N-bound ligands.

The average uranium−aryloxide bond lengths in complexes **2**−**9**, $d(U-O_{ArO})$, change with the oxidation state of the uranium ion: U^{VI} complexes **8** and **9** exhibit the shortest distance of ~2.100(2) Å, which is in the same range as found for other U^{VI} terminal oxo complexes.[2j] For U^V complexes **3**, **4**, and **5**, the bond distances are in the range of ~2.183 to ~2.215 Å, typical for $U-O_{ArO}$ bonds in U^V complexes.[2d,13] In case of dinuclear **7** and **6**, the bonds elongate with the degree of reduction from ~2.225(3) Å in **7** ($U^{IV/V}$) to ~2.370(2) Å in **6** ($U^{IV/IV}$). A similar trend for the average $U-N_{tacn}$ bond distances cannot be observed; the $U-N_{tacn}$ bond lengths vary from ~2.747 to ~2.867 Å for all complexes and thus are slightly longer than those found in other uranium complexes of the tacn chelate, which are in the range of 2.67 to 2.76 Å.[10,13,17] It is noteworthy that all of the new high-valent complexes, including the imido species **2** and the oxo complexes **3**−**9**, feature the ITI. Here the strongly π-donating terminal imido or oxo ligand is in plane with the three aryloxide ligands. Within this plane, the uranium−aryloxide bond trans to the terminal oxo/imido ligand is slightly shorter (~0.06 Å) than the two other cis $U-O_{Ar}$ bonds. The ITI is observed in the dinuclear complexes as well as in the mononuclear complexes to the same extent. In addition to the ITI, the inverse is also observed: the longest M−L distances are coordinated trans to each other (the longest M−L distance is trans to the tacn anchor).

Electrochemistry. Electrochemical data from cyclic, linear-sweep, and square-wave voltammetry were collected for all of the uranium complexes in THF or acetonitrile solutions, with ~0.1 M $[N(n\text{-}Bu)_4][PF_6]$ as the electrolyte and the ferrocene/ferrocenium (Fc/Fc^+) couple as an internal standard. In addition, both the free $({}^{nP,Me}ArOH)_3tacn$ ligand and 2.2.2-cryptand were investigated to demonstrate their redox inactivity. A summary of experimentally determined half-step potentials is given in the Supporting Information. In contrast to the complexes $[(({}^{R,R'}ArO)_3tacn)U^V(NTMS)]$ (R = *t*-Bu, Ad, diamantanyl; R′ = *t*-Bu, Me), the neopentyl derivative, U^V imido complex **2**, shows no redox chemistry in the accessible electrochemical window. This might be due to the different geometries (C_3 vs C_s) found in the *tert*-butyl and adamantyl complexes versus the neopentyl system studied here. The dinuclear bis(μ-oxo)-bridged complex **3**, however, shows a remarkablly rich and unique electrochemistry featuring two reversible redox events at half-wave potentials of $E_{1/2}$ = −0.08 and −1.53 V vs Fc/Fc^+ (see Figure 4). The more cathodic redox wave can be unambiguously assigned to the one-electron reduction of the U^V/U^V species to the mixed-valent U^{IV}/U^V complex. This couple also appears in the cyclic voltammogram (CV) of **7** ($E_{1/2}$ = −1.55 V vs Fc/Fc^+; see the Supporting Information), and similar reduction potentials for U^{IV}/U^V complexes are known (−1.25 to −1.81 V vs Fc/Fc^+).[18] The second redox wave at $E_{1/2}$ = −0.08 V vs Fc/Fc^+ is assigned to a one-electron oxidation to a U^V/U^{VI} complex, which is further confirmed by linear sweep. While the electrochemical reduction can be proved by a chemical reduction on a preparative scale, leading to isolable **7**, the chemical oxidation of **3** to yield the hypothetical mixed-valent $[U^V(\mu\text{-}O)_2U^{VI}]$ species has not yet been accomplished. Attempts to oxidize **3** with a large variety of oxidants and different stoichiometries led only to monomeric U^{VI} oxo complexes (vide supra). The large separation between the U^{IV}/U^V, U^V/U^V, and U^V/U^{VI} redox couples allows the equilibrium constant for the comproportionation to the U^V/U^V complex to be estimated. With $\Delta E_{1/2}$ = |1.45 V|, K_c is approximately 3.25×10^{24}, suggesting strong electronic communication between the uranium centers.[19] It is likely that the highly covalent U−O bonds in the bis(μ-oxo) diamond core support this electronic coupling, although short M···M distances (and their resulting M−M bonds) have also been implicated in strong interactions between two transition-metal centers. The large value of K_c may further explain the unusual stability of **3**, which is air-stable. A similar K_c value has been reported by Cummins and co-workers for a dinuclear nitrido-

dx.doi.org/10.1021/ja504528n | J. Am. Chem. Soc. 2014, 136, 11980−11993

bridged U^{IV}/U^{V} complex ($K_c \approx 5.6 \times 10^{17}$), for which a wave separation of $\Delta E_{1/2} \approx 1.05$ V between the U^{IV}/U^{IV}, U^{IV}/U^{V}, and U^{V}/U^{V} redox couples has been reported.[19b]

Interestingly, while treatment of **3** with excess KC_8 yields the doubly reduced U^{IV}/U^{IV} complex **6**, the second reduction, the U^{IV}/U^{V} to U^{IV}/U^{IV} redox couple, is not observed in the CV of **3**. Also, isolated complex **6** is electrochemically inert, showing neither reversible nor irreversible redox events in its CV. In view of the fact that in **6** two potassium cations are bound to one of the bridging oxo ligands and form multiple bonding interactions with the aryloxide pendant arms of each U^{IV} moiety, it is reasonable to assume that the chemically introduced potassium ions play a major role in the stabilization of **6**,[14] which may explain the different electrochemical and chemical behaviors. While mononuclear U^{VI} oxo complexes **8** and **9** show no reversible redox chemistry in the accessible electrochemical window, complexes **4** and **5** show one reversible redox event centered at $E_{1/2} = -0.18$ and -0.27 V vs Fc/Fc^+, respectively, consistent with reported redox potentials for the metal-centered U^{V}/U^{VI} redox couple (-0.11 to -0.19 V vs Fc/Fc^+).[2j,18] However, chemical oxidation of complex **4** with AgOTf resulted in ligand degradation and the formation of a U^{VI} uranyl complex coordinated by two triflate and three pyridine *N*-oxide ligands (see the Supporting Information).

Electronic Absorption Spectra. The UV/vis/NIR electronic absorption spectra of the dark-brown imido complex **2**, the yellow-orange terminal oxo complexes **4** and **5**, the dark-red-brown U^{V}/U^{V} complex **3**, the orange U^{IV}/U^{V} complex **7**, the pale-green U^{IV}/U^{IV} complex **6**, and the two black U^{VI} complexes **8** and **9** were measured in THF at different concentrations from 200 to 2500 nm at 25 °C. Generally, the electronic absorption spectra of complexes **2**–**7** can be divided into two regions: UV/vis and NIR. The UV/vis region (Figure 5A) shows intense and broad charge-transfer (CT) bands characteristic of $\pi \rightarrow \pi^*$ and $\pi \rightarrow nb_{5f}$ (nb = nonbonding) transitions and metal-centered 5f → 6d transitions above 40 000 cm^{-1} with molar extinction coefficients (ε) of 20–30 × 10^3 M^{-1} cm^{-1}.[20] The NIR region (Figure 5B) is dominated by metal-based f–f transitions with varying intensities and ε values that range from 10 to 600 M^{-1} cm^{-1} per uranium.

In the UV region, most of the complexes exhibit two similar features at ~250 and 300 nm with molar extinction coefficients of 20–30 × 10^3 M^{-1} cm^{-1} per uranium. In addition, dinuclear **3** and **7** show strong absorption into the visible spectrum below 600 nm with $\varepsilon \approx 3000$ M^{-1} cm^{-1} per uranium (at $\lambda \approx 483$ and 388 nm, respectively), whereas monomeric U^{V} complexes display only weak absorption below 450 nm. The U^{VI} complexes **8** and **9** absorb strongly over the entire range from 220 to 1280 nm, but no f–f transitions are observed, as expected for U^{VI}.

The metal-centered f–f transitions depend on the electronic configuration of the uranium ion. U^{V} is the simplest to understand since it possesses just one unpaired electron; hence, no electron–electron repulsion occurs. Absorptions with average molar extinction coefficients of ~50–100 M^{-1} cm^{-1} per uranium can be observed for the terminal oxo complexes **4** and **5** as well as for the dinuclear bis(μ-oxo) complexes **3** and **7** and are comparable to bands observed for the terminal oxo complexes $[((^{t\text{-Bu},t\text{-Bu}}ArO)_3tacn)U^{V}(O)]$, $[((^{Ad,t\text{-Bu}}ArO)_3tacn)U^{V}(O)]$, and recently reported $K[UO(Si(O\text{-}t\text{-}Bu)_3)_4]$.[2n,13] The wider range of 840–1670 nm for **4**, compared with 880–1610 nm for **5**, suggests a slightly stronger ligand field in **4**, which

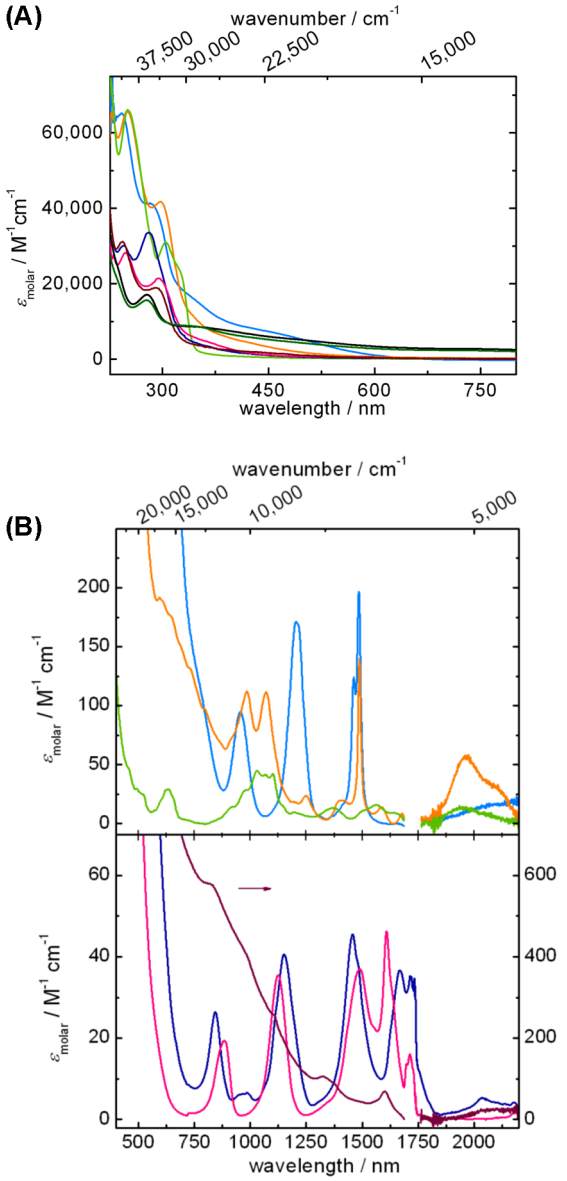

Figure 5. (A) UV/vis absorption spectra of **2** (purple), **3** (blue), **4** (dark blue), **5** (pink), **6** (green), **7** (orange), **8** (black), and **9** (dark green). (B) NIR absorption spectra: (top) **3**, **6**, and **7**; (bottom) **2**, **4**, and **5**. Extinction coefficients per uranium center are reported.

produces a larger splitting of the states. In stark contrast to the U^{V} oxo complexes, U^{V} imido compound **2** shows one broad absorption band, spanning from ~750 to 1700 nm, with some less-resolved superimposed features. The spectral shape and intensity ($\varepsilon \approx 70$–580 M^{-1} cm^{-1}) is reminiscent of the spectrum of the $[((^{t\text{-Bu},t\text{-Bu}}ArO)_3tacn)U^{V}(NMes)]$ and $[((^{Ad,t\text{-Bu}}ArO)_3tacn)U^{V}(NMes)]$ complexes[13] and to other reported U^{V} imido complexes.[18,21]

For the purposes of interpreting the NIR spectra, the U^{V} oxo complexes may be viewed as distorted octahedral complexes with the tacn anchor occupying a single coordination site, as noted earlier. Of these complexes, **7** has the least distorted $[U(\mu\text{-}O)_2U]$ core, with U–O distances of 2.11 and 2.17 Å; the $U\text{–}O_{ArO}$ distances are somewhat longer at 2.25 Å. Complex **3** has a more distorted $[U(\mu\text{-}O)_2U]$ core with U–O distances of 2.07 and 2.20 Å, and **4** and **5** are strongly distorted with a short terminal oxo distance of 1.86 Å. These four U^{V} complexes form

dx.doi.org/10.1021/ja504528n | J. Am. Chem. Soc. 2014, 136, 11980–11993

a series in which the relatively symmetric $[U(\mu\text{-}O)_2U]$ diamond core in **7** begins to distort in **3**, with its shorter U−O bond finally becoming the terminal oxo ligand in **4** and **5**.

The NIR spectra of pseudo-octahedral uranium complexes have previously been described,[22] and the bonding has been interpreted by using a crystal field model.[23] Like **3**−**5**, dianionic $[UOX_5]^{2-}$ possesses a short U−O bond in a distorted octahedral coordination environment. The other related complex is the anion $[U(O\text{-}t\text{-}Bu)_6]^-$, which displays U−OR bond lengths of 2.05 to 2.24 Å, very similar to those observed here.[24] Therefore, the NIR spectrum of **7** should be expected to be similar to that of $[U(O\text{-}t\text{-}Bu)_6]^-$, and the spectra of **3**−**5** should be related to that of **7** in the same way that the spectrum of $[UOX_5]^{2-}$ is related to that of $[UX_6]^-$.

The splitting of the f orbitals in a pseudo-octahedral f^1 complex can be described as shown in Figure 6, following the

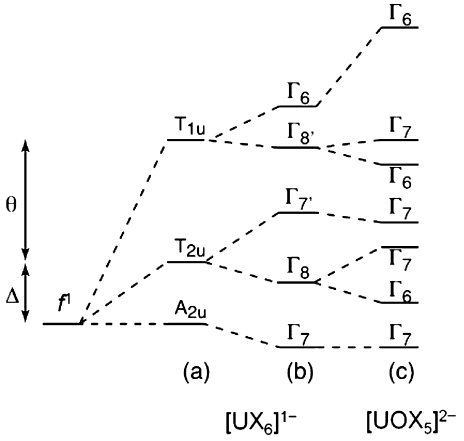

Figure 6. Splitting of an f^1 system due to (a) the O_h ligand field of $[UX_6]^-$, (b) the effect of spin−orbit coupling, and (c) the effect of replacing X with a terminal oxo ligand. Diagram after Selbin and Sherrill.[23]

scheme developed by Selbin and Sherrill.[23] In contrast to the complexes described by Selbin and Sherrill, the f_{xyz} (a_{2u}) orbital participates in bonding in **3**−**5** and **7** (primarily with the tacn amine nitrogen atoms), so the A_{2u} state in **3**−**5** and **7** is antibonding rather than nonbonding. With the labels for octahedral symmetry (Figure 6b), the NIR spectrum of **7** may be assigned by reference to the spectrum of $[U(O\text{-}t\text{-}Bu)_6]^-$. The sharp feature at 1487 nm is the $\Gamma_7 \rightarrow \Gamma_{7'}$ transition (6725 cm^{-1}), the absorption bands at 984 and 1072 nm are the two branches of the $\Gamma_7 \rightarrow \Gamma_{8'}$ transition (9745 cm^{-1}) (this peak is always split in octahedral U^V complexes), and the shoulder at 795 nm is assigned to the $\Gamma_7 \rightarrow \Gamma_6$ transition (12 580 cm^{-1}).

In going from **7** to **3** to **4** and **5**, one bridging oxo ligand becomes the short terminal oxo ligand, which is analogous to moving from $[UX_6]^-$ to $[UOX_5]^{2-}$. Consequently, the Γ_6 state in **7** increases in energy in **3**, forming the shoulder at 750 nm, and is unobserved in **4** and **5** (it should appear at ∼625 nm but is obscured by the CT bands). The $\Gamma_{8'}$ feature at around 1000 nm in **7** splits in **3**−**5** as the distortion increases, forming a Γ_6 peak at ∼1150 nm and a Γ_7 peak at ∼900 nm. The energy of $\Gamma_{7'}$ is roughly in the same region as observed in all complexes at ∼1450 nm. A new peak appears for **4** and **5** at ∼1600 nm, which is presumably the Γ_7 peak produced by splitting of the Γ_8 peak in **7**, which is in the IR. Interestingly, all of the transitions in Mazzanti's closely related $K[UO(Si(O\text{-}t\text{-}Bu)_3)_4]$ appear in the NIR, thus implying a stronger crystal-field splitting in this complex.[2n]

On the basis of the assigned energies of the $\Gamma_{7'}$, $\Gamma_{8'}$, and Γ_6 states of **7** and its average *g* value (1.080), the crystal field of **7** may be modeled as previously done for $[U(O\text{-}t\text{-}Bu)_6]^-$ (Table 3). The fitting parameters are the spin−orbit coupling

Table 3. Summary of U^V Transitions and Crystal Field Parameters for 7 and $Li(Et_2O)[U(O\text{-}t\text{-}Bu)_6]$[a]

	7	$Li(Et_2O)[U(O\text{-}t\text{-}Bu)_6]$[b]
$\Gamma_{7'}$ (exp) (cm^{-1})	6725	7094
$\Gamma_{7'}$ (calc) (cm^{-1})	6621	7116
$\Gamma_{8'}$ (exp) (cm^{-1})	9745	11221
$\Gamma_{8'}$ (calc) (cm^{-1})	10140	11235
Γ_6 (exp) (cm^{-1})	12580	13261
Γ_6 (calc) (cm^{-1})	12302	13414
g (exp)	−1.080	−0.730
g (calc)	−1.083	−0.719
ζ (cm^{-1})	1878(150)	1884(110)
θ (cm^{-1})	4622(700)	4670(605)
Δ (cm^{-1})	2166(270)	3779(250)

[a]Standard deviations of the parameters are given in parentheses. [b]See ref 5a.

parameter ζ and two splitting parameters θ and Δ, illustrated in Figure 6. ζ was almost identical to that of $[U(O\text{-}t\text{-}Bu)_6]^-$, which implies that bonding is equally covalent in the two complexes. Likewise, θ, which is essentially the destabilization of the f orbitals due to σ bonding, is almost identical in the two complexes. On the other hand, Δ, which is the destabilization of the f orbitals due to π bonding, is much smaller in **7** (2166 cm^{-1}) than in $[U(O\text{-}t\text{-}Bu)_6]^-$ (3779 cm^{-1}). This difference may be rationalized by noting that each *tert*-butoxide ligand can form two π bonds with the U center but the aryloxide and bridging oxo ligands may only form a single π bond with each uranium center. Overall, the electronic structure and bonding in **7** are very similar to those in $[U(O\text{-}t\text{-}Bu)_6]^-$ with the exception that π bonding is somewhat weaker in **7**.

Although the f−f transitions in **2** are significantly more intense (∼10 times) than for the U^V complexes **4** and **5**, their CT transitions are equally intense, which is in contrast to recent reports of Kiplinger and co-workers.[25] The comparatively high molar extinction coefficients for these U^V complexes, in contrast to other U^V compounds such as pseudo-octahedral U^V halide complexes (ε = 5−22 M^{-1} cm^{-1}), may arise from the low C_s symmetry, leading to a relaxation of the electric dipole selection rules. The same behavior was observed for Kiplinger's complexes, which have ε values ranging from ∼100 to 400 M^{-1} cm^{-1}.[26] Also, the nature of the uranium−ligand bond significantly affects the intensities of the absorption bands. While simple σ-donor ligands typically lead to low intensities, more covalently bound π-donor ligands, such as complexes with terminal oxo and imido ligands, possess larger extinction coefficients as a result of orbital mixing and relaxation of Laporte's rule ("intensity stealing").[27]

The most salient feature in the spectrum of **6** is the lack of the distinctive U^V transitions observed in **3**−**5** and **7**. This is not only immediately indicative of the complete reduction of pentavalent **3** and mixed-valent **7** to fully tetravalent **6** but is in good agreement with the structural observation of a symmetric $[U^{IV}(\mu\text{-}O)_2U^{IV}]$ core with relatively long but equal U−O bond distances, indicating weaker U−O bonds with little to no

dx.doi.org/10.1021/ja504528n | J. Am. Chem. Soc. 2014, 136, 11980−11993

double-bond character. Instead, the spectrum of **6** is reminiscent of those for "typical U^{IV} complexes" of the tacn and single N-anchored tris(aryloxide) complexes, featuring a large number of low-intensity f−f transitions over the entire spectral range. The U^{IV} ion with its $5f^2$ electron configuration experiences electrostatic repulsion of the two f electrons as well as significant spin−orbit coupling, which leads to a large number of levels within the $^3H_4$ ground state. In addition, depending on the symmetry and crystal-field strength, the levels are further split into $(2J + 1)$ states. In U^{IV}, the crystal-field splitting is typically between 100 and 2000 cm^{-1},[20] which is on the same order of magnitude as the spin−orbit coupling energy. This leads to a significant mixing of states and consequently a large number of f−f transitions in the visible to NIR region. Accordingly, **6** possesses several unresolved bands from 450 to 1950 nm with low molar extinction coefficients of 10−50 M^{-1} cm^{-1}.[28]

IR Spectroscopy. The nature of the $U-O_{oxo}$ bonds in complexes **3**−**9** was further probed by IR and Raman vibrational spectroscopy. It should be noted that employing $C^{18}O_2$ in the multiple-bond metathesis reaction enabled the synthesis and isolation of the ^{18}O-labeled bis(μ-oxo)-bridged dinuclear analogues of **3**, **6**, and **7** and allowed for the first time the unambiguous assignment of the vibrational signature of the [U(μ-O)$_2$U] diamond core structural motif.

The IR spectra, recorded on solid samples (KBr pellet; see the Supporting Information), are all dominated by the spectrum of the relatively complex hexadentate chelating ligand system in [((^{nP,Me}ArO)$_3$tacn)U(L)]. Consequently, all of the complexes show very similar vibrational spectra, except for a single absorption band in the fingerprint region at 748 cm^{-1} for **4** and 741 cm^{-1} for **5**, respectively (see the Supporting Information). This feature cannot be observed in complexes **2**, **3**, and **6**−**9** and is therefore assigned to the terminal oxo−uranium stretching vibration, ν(U═O). Although labeling studies were not performed on **4** and **5** (these complexes were not synthesized from CO_2), the energy of the assigned ν(U═O) peak is in good agreement with literature reports.[2c,h] Unambiguous identification of the metal−oxygen bond stretching frequencies in the [U(μ-O)$_2$U] diamond core of dinuclear complexes **3**, **6**, and **7**, as well as the U═O group in their mononuclear oxidation products **8** and **9**, was achieved through the use of isotopic labeling with $C^{18}O_2$ (95% enriched in ^{18}O). Thus, comparison of the parent complexes with their ^{18}O-labeled isotopomers **3***, **6***, **7***, **8***, and **9*** revealed two strong isotope-sensitive bands between 500 and 648 cm^{-1} (see the Supporting Information). These vibrational bands were assigned to the symmetric stretching and symmetric deformation vibrations. Similar values between 600 and 900 cm^{-1} have been reported for transition-metal complexes containing the [M(μ-O)$_2$M] diamond core moiety (M = Mn, Co, Os).[29] For the mononuclear U^{VI} oxo complexes **8** and **9**, a shift of one vibrational band from 829 to 818 cm^{-1} and 826 to 822 cm^{-1} for the isotopomers **8*** and **9***, respectively, was observed. These values are comparable to those reported for the terminal U^{VI} oxo complexes [((Me$_3$Si)$_2$N)$_3$$U^{VI}$O(X)] (X = F, Cl, Br) reported by Schelter and co-workers (ν(U═O) = 859−882 cm^{-1}).[2m] The results obtained from IR vibrational spectroscopy agree well with the ones obtained from X-ray crystallographic studies and verify that the overall U═O bond order is lowered from the terminal oxo U^{VI} (1.794(2), 1.791(6), and 1.800(6) Å) to the terminal oxo U^{V} (1.8561(18), 1.8586(18), and 1.860(2) Å) to the dinuclear bis(μ-oxo)-bridged complexes.

Raman Spectroscopy. Raman spectroscopy measurements for all of the labeled and unlabeled complexes were conducted in the solid state at room temperature. Because of strong emissions for all of the complexes except for **3** and its ^{18}O isotopomer **3***, no meaningful Raman spectra could be obtained. For **3** and **3***, however, a set of features are evident in the spectra, but only one shift is sensitive to ^{18}O substitution, moving from 622 to 584 cm^{-1} (588 cm^{-1} calculated for a simple U−O harmonic oscillator) and assigned to the "breathing" mode of the diamond core moiety (see the Supporting Information). Similar values and assignments can be found in the literature for [M(μ-O)$_2$M] diamond cores in transition-metal complexes. For example, Tolman and co-workers synthesized [Cu(μ-O)$_2$Cu] complexes with Raman shifts from 604−647 cm^{-1} for the unlabeled complexes and 570−624 cm^{-1} for the ^{18}O-labeled complexes.[30] Further complexes show similar shifts for the unlabeled (700−590 cm^{-1}) and ^{18}O-labeled (634−560 cm^{-1}) [M(μ-O)$_2$M] diamond core moiety (M = Fe, Mn, Ni).[31]

Magnetism. Until recently, the magnetism of U^{V} compounds has not been extensively investigated because of the difficulty in preparing complexes in this oxidation state. This has been particularly true for coordination complexes of low symmetry and for magnetically coupled systems.[6e] More recently, the development of novel synthetic routes to stable U^{V} complexes has led to an expansion in the studies of the magnetism of this oxidation state.[2f,5a,c,6f,32] Nevertheless, exchange-coupled systems remain rare.[6] Thus, the complexes described in this paper offer a unique opportunity to study the magnetic properties of this novel series of dinuclear uranium coordination complexes with similar uranium coordination environments. Reproducible temperature-dependent and field-dependent magnetization data were collected for several isolated and independently synthesized samples. Even in analytically pure samples, all of the complexes exhibit small amounts of an unidentified paramagnetic impurity. These ubiquitous impurities may occur from minute uncoupled impurities (for the dinuclear complexes), ferrites (especially magnetite) from stainless steel lab equipment, and/or defects at the surface of the microcrystallites.[33] The presence of impurities is mainly noticeable in the low-temperature (T < 14 K) magnetic susceptibility data for **3** and **6**, since both of these complexes have very small magnetic moments at low temperature.

The magnetic susceptibilities of these complexes are best understood using the van Vleck equation (eq 1),

$$\chi = \frac{\sum_j \chi_j e^{-E_j/kT}}{\sum_j e^{-E_j/kT}} \tag{1}$$

where

$$\chi_j = N\left(\frac{\mu_B{}^2 g^2 S(S+1)}{3kT} - \alpha\right)$$

and

$$\alpha = \sum_{j\neq k} \frac{2|\langle \phi_k|\mathbf{L} + 2\mathbf{S}|\phi_j\rangle|}{E_j - E_k}$$

dx.doi.org/10.1021/ja504528n | J. Am. Chem. Soc. 2014, 136, 11980−11993

in which χ_{mol} is the magnetic susceptibility of the complex, χ_ϑ is the magnetic susceptibility of a thermally occupied state at energy E_j, the α term is the temperature-independent paramagnetism (TIP) due to low-lying excited states, and the other symbols have their usual meanings.[34] The magnetic susceptibility of a given complex is just the Boltzmann average of the susceptibilities of the occupied states, and the susceptibility of each state has a temperature-dependent term proportional to g^2 and a temperature-independent term that is inversely proportional to the energies of the excited states. In uranium complexes, some excited states are typically at low energy and become thermally populated below 300 K. In addition, the TIP term α is often large in these systems as a result of the low energies of the excited states. When the magnetic susceptibility is plotted as χT versus T, the occupancy of the low-lying states is often discernible by the change in the slope of χT versus T. At low temperatures, where only a single state is occupied, χT is linear in T. The TIP term can be determined from the slope, and the average value of g can be determined by extrapolating χT to 0 K (χT at 0 K). As the temperature increases and low-lying states become thermally populated, the slope of χT versus T decreases (the TIP terms of the ground and excited states cancel), and the slope of χT versus T changes (the plot curves) until the occupied states are in thermal equilibrium, at which point χT versus T is again linear. If the total splitting of the f orbitals by the crystal field is significantly smaller than kT at room temperature, all of the states in the ground multiplet (e.g., $^2F_{5/2}$ for U^V) are in thermal equilibrium, and the magnetic moment may be compared to that of the free ion.

The strength of the crystal field has a large effect of the magnetic susceptibility of the complex. If the ligands create a crystal field that is large compared to kT at 300 K, only the lowest-lying f states will be occupied, and the magnetic susceptibility will be significantly different from that of the free ion. If this is the case, a plot of χT versus T will be significantly temperature-dependent at 300 K because of TIP created by slightly higher lying excited states. A strong crystal field will also result in mixing of the lowest-lying free-ion states (e.g., $^2F_{5/2}$ and $^2F_{7/2}$ for U^V), resulting in further deviation of the magnetic moment from that of the free ion. Covalent interactions also affect the magnetic moment by reducing the orbital angular momentum of the complex, which decreases both g and α in eq 1.[35]

Magnetic moments at room temperature and extrapolated to 0 K are given in the Table 4 for complexes **2**–**7**. The magnetic susceptibilities of complexes **4** and **5** are typical of U^V complexes stabilized by oxo ligands (see the Supporting Information).[2e,f,13] In all of the complexes, the magnetic moment at 300 K is significantly reduced from the free-ion moment of 2.54μ_B for $^2F_{5/2}$. Also, χT has substantial temperature dependence at 300 K, which is consistent with the large crystal-field splitting observed in the NIR. In **4**, χT is linear in T from 0 to 20 K, at which point the slope changes until χT is again linear in T from 150 to 300 K, which indicates that the first excited state is ~50 K (35 cm^{-1}) above the ground state and that no other low-lying excited states become populated below 300 K. In **5**, on the other hand, χT is linear in T from 5 to 300 K with a slight deviation below 5 K. In this case, either the first excited state is very low in energy and is in thermal equilibrium with the ground state at 5 K or the first excited state does not become significantly populated below room temperature. On the basis of the relatively large splitting of the f orbitals observed in the NIR (>5000 cm^{-1}) relative to kT at 300 K (209 cm^{-1}), the latter explanation seems more likely. The ground states of these complexes have magnetic moments similar to those of octahedral $[UX_6]^-$ complexes, which vary from 0.63μ_B for $[U(OR)_6]^-$ to 1.24μ_B for $[UR_6]^-$ as determined from the g values of their ground states.[5a] This similarity supports the analogy with octahedral f^1 ions presented when discussing the electronic spectra and suggests that the half-occupied orbital is largely f_{xyz} in character. The lack of low-lying states in **5** is also consistent with the picture.

The three dinuclear complexes (**3**, **6**, and **7**) show remarkably different magnetic behavior, as is clearly observable in the plots of χ versus T and χT versus T (Figure 7, Table 4).

Table 4. Magnetic Moments of the Complexes per Uranium at 300 K and Values Extrapolated to Zero K

complex	μ_{eff} at 0 K (μ_B/U)	μ_{eff} at 300 K (μ_B/U)
2	1.22	1.89
3	0.14	1.66
4	0.75	1.70
5	0.83	1.68
6	0.13	2.73
7	0.74	2.26
7- $^1/_2$ **6**	1.00	1.76

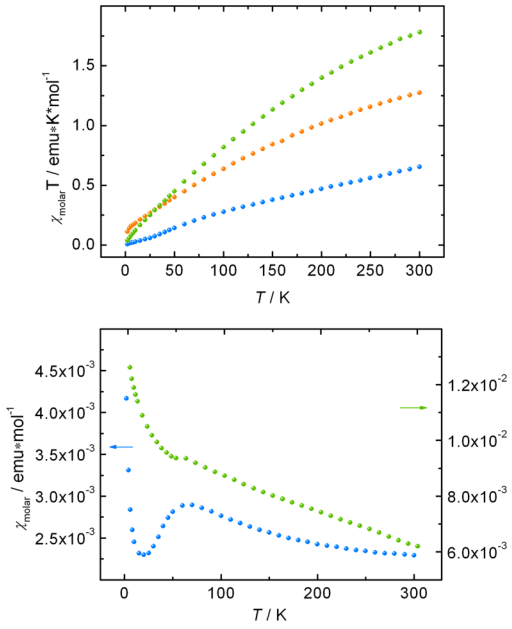

Figure 7. Temperature-dependent magnetic susceptibility data for **3** (blue), **6** (green), and **7** (orange) shown as plots of χT vs T (top) and χ vs T (bottom). For the χ vs T plot, the scale for **3** is on the left and the scale for **6** is on the right.

The χ versus T plot for complex **3** exhibits the magnetic behavior of an antiferromagnetically coupled dinuclear complex with a Néel temperature (T_N) of approximately 70 K. The (reproducible) upturn in susceptibility below 14 K is attributed to the presence of paramagnetic impurities. At room temperature, **3** has a magnetic moment per U that is comparable to those of the other U^V complexes.[2e,f,13] Interestingly, the χT versus T plot of **3** is linear from 100 to 300 K, which suggests that no further states become thermally populated over this

dx.doi.org/10.1021/ja504528n | J. Am. Chem. Soc. 2014, 136, 11980–11993

range. The strong temperature dependence of χT for **3** at 300 K suggests that only the lowest crystal-field states of each ion—possibly only a single crystal-field state—are populated below room temperature, which is consistent with the NIR spectrum of this ion. Magnetic exchange in this complex will be addressed below.

The magnetic susceptibility of the doubly reduced complex **6**, $[U^{IV}(\mu\text{-}O)_2U^{IV}]$, shows no evidence of exchange coupling because of its non-magnetic ground state at low temperatures. Instead, **6** displays characteristic behavior for isolated tetravalent U^{IV} complexes.[2g,36] Specifically, χT for **6** is linear to 70 K with χT at 0 K approximately equal to zero, which implies that the g value of the ground state is zero. In addition, the χ versus T plot of **6** displays a plateau below 70 K, which is masked by the presence of paramagnetic impurities (vide supra). To estimate the energy gap between the ground and excited states, it is assumed that an excited-state population of less than 5% leads to no change in magnetic susceptibility.[37] When the Boltzmann distribution is applied, a state energy gap of ~125 cm^{-1} can be expected.[37,38]

The free-ion ground state for U^{IV} is $^3H_4$, which is split by the ligand field into three non-Kramers doublet states and one singlet state. The singlet state has a g value of zero and displays only TIP, which is consistent with the ground-state magnetic susceptibility observed for **3**. In octahedral crystal fields, U^{IV} displays a singlet ground state,[39] which further supports the postulate that these complexes may be viewed as distorted octahedra, at least from the perspective of their electronic structures. A singlet ground state in **6** is consistent with the observed lack of coupling in this molecule, since singlet states have an effective spin, $\hat{\mathbf{S}}$, equal to zero and do not participate in exchange coupling. As with the other complexes, χT for **6** is strongly temperature-dependent at 300 K, which is consistent with the large crystal-field splitting observed in its NIR spectrum.

In agreement with its electronic absorption spectrum (vide supra), the mixed-valent U^{IV}/U^{V} complex **7** shows magnetic behavior reminiscent of both U^{IV} and U^{V}. In **7**, χT is linear in T from 6 to 100 K with a small deviation below this value. Therefore, only a single state is (or two almost degenerate states are) thermally occupied over this range, which is consistent with the behaviors of both **6** and with the monomeric U^{V} species **5**. At 300 K, as one might expect, the magnetic moment is intermediate between those of the U^{IV} complex **6** and the monomeric U^{V} complexes. For **7**, χT does not become linear at higher temperature, most likely because of the changing thermal populations of the low-lying states, which is similar to the behavior of **6**. As with the other complexes, χT is strongly temperature-dependent at 300 K, which suggests that only the lowest-lying states are thermally occupied and is consistent with the large splitting of the f states observed in the NIR.

The Néel temperature of **3** (T_N = 70 K) is considerably higher than typically observed for U^{V} complexes.[6a,e,f,40] Only T_N of the U^{III} inverse sandwich complex described by Cummins and co-workers is larger at 110 K. The exchange coupling in **3** may be quantified if the magnetic anisotropy and magnetic susceptibility of an isolated magnetic ion (diamagnetic substitute) are available.[41] Here the ideal diamagnetic substitute would be the analogous complex with one of the uranium atoms replaced by protactinium,[42] which is prohibitively difficult. The role of the diamagnetic substitute is to account for the effect of the crystal field on the magnetic susceptibility of the ions in the coupled pair. Therefore, a complex with a structure similar to that of **3** but without a neighboring magnetic ion could also be used as the diamagnetic substitute. While **4** and **5** are similar to **3**, the uranium terminal oxo distances in **4** and **5** are considerably shorter than the short U–O bond in **3**. On the other hand, the structure of **7** is quite similar to that of **3** and could be a useful diamagnetic substitute if one can account for the susceptibility of the U^{IV} center.

Since the U^{IV} center in **7** should have an electronic structure similar to those of **6**, it is possible that the latter complex can be used to correct for the presence of the U^{IV} center in **7** by simply subtracting half of the susceptibility of **6** from that of **7**. While this approach would fail if the uranium centers in **7** were magnetically coupled, the U^{IV} center in **7** should have the same singlet ground state as in **6** and therefore should not be magnetically coupled to the U^{V} center in **7**. As shown in Figure 8, this procedure does result in the typical magnetic susceptibility of a U^{V} ion. χT is linear over the entire temperature range, which is consistent with occupancy of only a single crystal-field state below 300 K, as seen with mononuclear **5**. The data in Figure 8 represent the magnetic susceptibility of an isolated U^{V} center in **7** and **3**. In addition to the magnetic susceptibility of the diamagnetic substitute, its magnetic anisotropy is needed and may be obtained from the EPR spectrum. As shown in Figure 9, at 2 K the mixed-valent U^{IV}/U^{V} complex **7** displays the rhombic EPR spectrum of a low-symmetry complex, and its anisotropy (γ) is given by g_{min}/

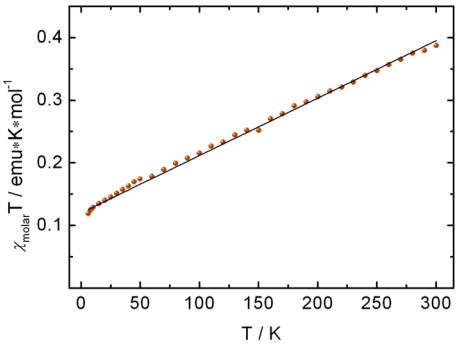

Figure 8. Magnetic susceptibility of **7** minus half of the magnetic susceptibility of **6**. The linear fit to the data is indicated by the solid line.

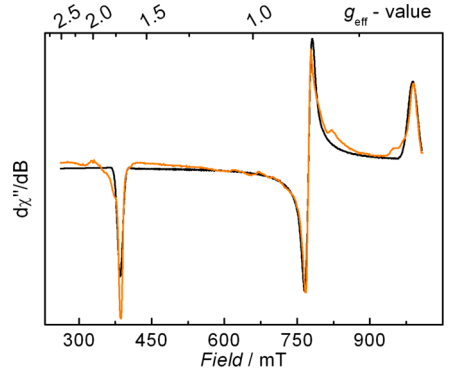

Figure 9. X-band EPR spectrum of a solid sample of **7** (orange) at 2 K and simulation (black) with g_1 = 1.712, g_2 = 0.851, and g_3 = 0.666. Experimental conditions: ν = 9.21994 GHz; P = 10 mW; modulation amplitude = 10 G.

dx.doi.org/10.1021/ja504528n | J. Am. Chem. Soc. 2014, 136, 11980–11993

g_{max} = 0.39. The magnetic moment of the ground state may be determined from the EPR spectrum using the relation $4\mu_{eff}^2 = (g_1^2 + g_2^2 + g_3^2)$. The resulting value, μ_{eff} = 1.01μ_B, may be compared with value of μ_{eff} at 0 K determined from a linear fit of the data shown in Figure 8 (1.00μ_B). The excellent agreement between these values supports the notion that the magnetic susceptibility of the U^V center in **7** may be modeled by subtracting half the susceptibility of **6** from that of **7**.

In **3**, with strong antiferromagnetic exchange, the standard Heisenberg–Dirac–van Vleck (HDVV) spin Hamiltonian can be applied to the spins. The HDVV spin Hamiltonian is given by

$$\mathcal{H} = -2\mathcal{J}\mathbf{S}_1\cdot\mathbf{S}_2$$

where $2\mathcal{J}$ is the difference in energy between the singlet and triplet states and $\mathbf{S}_i$ is the spin of the ith electron. In molecules such as **3** with unquenched orbital angular momentum **L** and strong spin–orbit coupling, the total angular momentum **J** rather than **S** is applicable, and the system is described using an effective spin $\hat{\mathbf{S}}$ that accounts for the degeneracy of the state and is related to the angular momentum by the g values and the Landé factor.[43] Since the states of the individual U centers in **3** are Kramers doublets, $\hat{S} = {}^1/_2$ and the resulting effective spin Hamiltonian $\hat{H}$ is anisotropic:

$$\hat{H} = 4J_\perp\hat{S}_{\perp 1}\hat{S}_{\perp 2} + 2J_\parallel\hat{S}_{\parallel 1}\hat{S}_{\parallel 2}$$

where $\hat{J}_\parallel = (g_\parallel/g_J)^2(g_J - 1)^2\mathcal{J}$ and $\hat{J}_\perp = (g_\perp/g_J)^2(g_J - 1)^2\mathcal{J}$, which leads to $\hat{J}_\perp = (g_\perp/g_\parallel)^2\hat{J}_\parallel$. In other words, the magnetic anisotropy of the isolated ion produces highly anisotropic coupling of the effective spins.

In contrast to the anisotropy, the paramagnetic impurity is easy to take into account. In this case, the magnetic susceptibilities of the three lowest data points were fit to the Curie–Weiss equation, $\chi = C/(T - \theta)$, to determine θ, which was held constant. The value of C was allowed to vary in the fit to account for the paramagnetic impurity. In addition to the Curie constant of the impurity, the parameters used in the fit were $\mathcal{J}$ (the HDVV coupling constant) and w (a weighting factor applied to the susceptibility of the diamagnetic substitute to account for weighing errors). The model also used the linear fit to the data in Figure 8 to represent the magnetic susceptibility of an isolated U^V center. In the modeled magnetism of **3** shown in Figure 10, the magnetic susceptibility of the ferromagnetically coupled state was calculated using the linear fit in in Figure 8; the magnetic susceptibility of the antiferromagnetically coupled ground state is zero.

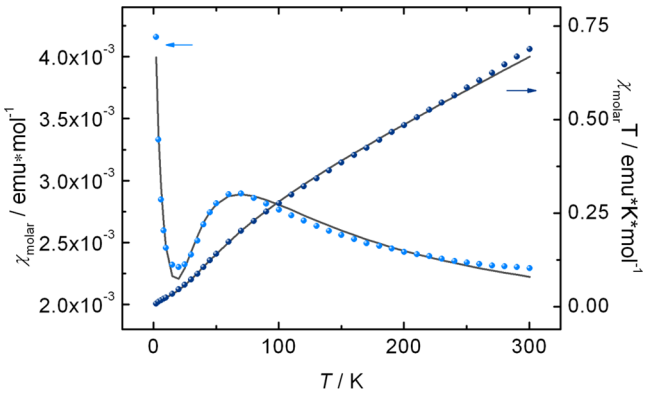

Figure 10. Fitting of the temperature-dependent SQUID magnetization data for **3** with γ = 0.39 (from EPR), C = 0.044, w = 0.91, and $\hat{J}_\parallel = -65$ cm^{-1} ($\hat{J}_\perp = \gamma^2\hat{J}_\parallel = -10$ cm^{-1}).

The fit of the susceptibility of **3** using this approach is shown in Figure 10. The value of $2\mathcal{J}$ determined for **3** (1650 cm^{-1}) likely has no physical significance in and of itself because the large crystal field in this complex mixes the $^2F_{5/2}$ and $^2F_{7/2}$ states, so g_J is not that of either state. The values of $\hat{J}_\parallel$ and $\hat{J}_\perp$, −65 and −10 cm^{-1}, respectively, are still meaningful: $-2\hat{J}_\parallel$ is the observed singlet–triplet gap when the magnetic field is parallel to the axis with g = 1.71, and $2\hat{J}_\perp$ is the gap when the magnetic field is perpendicular. While it would be interesting to relate $\hat{J}_\parallel$ and $\hat{J}_\perp$ to a structural feature of **3**, this cannot be done without knowing the alignment of $g_\parallel$ relative to the molecule. In any case, the magnetic anisotropy in **3** is mainly an artifact of unquenched orbital angular momentum and strong spin–orbit coupling.

The T_N of 70 K for **3** is the second highest value reported for a uranium compound; only the T_N of 110 K observed for the arene-bridged U^{III} dimer reported by Cummins and co-workers is greater.[6i,9] However, only few solid-state materials, such as UCl_3 and UBr_3, with ordering temperatures of 22 and 15 K, respectively, have been studied in detail.[44] Few coordination complexes of U^V that show f^1–f^1 coupling between the uranium centers via the bridging ligand are known. In 1990, Rosen, Andersen, and Edelstein presented the first U^V/U^V complex showing antiferromagnetic coupling, $[\{(MeC_5H_4)_3U\}_2(\mu\text{-}1,4\text{-}N_2C_6H_4)]$.[6e] In this case, the U^V centers are bridged by 1,4-diimidobenzene, which yields a T_N of ∼20 K. In 2008, Mazzanti and co-workers reported the dimeric U^V uranyl complex $[UO_2(dbm)_2K(18C6)]_2$, in which two uranyl oxos act as bridging ligands.[6c] Herein $T_N \approx 5$ K, suggesting weak antiferromagnetic exchange coupling; slightly stronger coupling was observed in a structurally related trimeric complex with T_N = 10 K.[40] In 2009, Boncella and co-workers reported exchange coupling in an imido analogue of U^V uranyl in which T_N = 13 K, compared with ∼5 K for the related U^V uranyl analogue.[6d] Recently, in 2012, Love, Arnold, and co-workers studied the dinuclear complex $[(Me_3SiOUO)_2(L)]$ (L = polypyrrolic macrocycle) and reported a relatively strong antiferromagnetic coupling, with an ordering temperature of 17 K.[6f] Ordering temperatures in a comparable temperature range to that of **3** (70 K), however, only occur in solid-state uranium compounds, including UO_2 (28.7 K), UN (53 K), and UBi (285 K).[45]

CONCLUSIONS

In 2008, we reported the synthesis of mononuclear U^V terminal oxo complexes via multiple-bond metathesis of a high-valent U^V imido complex with CO_2.[13] With the introduction of the neopentyl-derivatized tris(aryloxide) tacn chelate $(^{nP,Me}ArO)_3tacn^{3-}$ (instead of ortho *tert*-butyl or adamantyl substituents),[10] the U^V imido $[((^{nP,Me}ArO)_3tacn)\text{-}U^V(NMes)_{eq}(py)_{ax}]$ (**2**) not only shows an entirely different and surprising coordination mode but also leads to a "different" reaction product when exposed to an atmosphere of CO_2. The multiple-bond metathesis reaction of the imido complex with CO_2 still eliminates isocyanate, but the terminal oxo complex formed in situ dimerizes to yield the principal dinuclear complex **3** with a $[U^V(\mu\text{-}O)_2U^V]$ diamond core structural motif. This reaction selectivity is likely due to the more flexible neopentyl substituents and to additional π-C–H interactions of the phenolate rings and the neopentyl groups, which stabilize the dinuclear diamond core.[10] Complex **3** can be reduced by one or two electrons to yield the mixed-valent U^{IV}/U^V bis(μ-

dx.doi.org/10.1021/ja504528n | J. Am. Chem. Soc. 2014, 136, 11980–11993

oxo) complex $[K(crypt)][\{((^{nP,Me}ArO)_3tacn)U^{IV/V}\}_2(\mu\text{-}O)_2]$ (**7**) and the U^{IV}/U^{IV} bis(μ-oxo) complex $K_2[\{((^{nP,Me}ArO)_3tacn)U^{IV}\}_2(\mu\text{-}O)_2]$ (**6**), respectively. The convenient synthesis via U═NR/CO_2 multiple-bond metathesis provides access to the ^{18}O-labeled isotopomers by the use of ^{18}O-labeled $C^{18}O_2$. Thus, for the first time, the unambiguous assignment of the vibrational signature of the $[U(\mu\text{-}O)_2U]$ diamond core structural motif in **3**, **6**, and **7** has been accomplished. Oxidation of the dinuclear U^V/U^V complex invariably gave mononuclear U^{VI} oxo complexes, independent of the coordination chemistry of the oxidant anion. Oxidation of **3** led exclusively to formation of monomeric U^{VI} oxo complexes with the counterion either coordinated (triflate) or not (SbF_6^-), depending on the oxidizing agent. Additionally, two mononuclear U^V oxo complexes were synthesized independently. The UV/vis/NIR electronic absorption spectra of the pentavalent complexes **3**−**5** can be understood by considering the tacn anchor to be a single ligand. This assumption means that the coordination spheres of these complexes can be considered distorted octahedra. In this symmetry, the half-occupied orbital is f_{xyz}, and the f−f transitions may be assigned by analogy to the simple and well-understood $[UX_6]^-$ and $[UOX_5]^{2-}$ systems. The energies of the low-lying f−f transitions show that the splitting of the f orbitals due to their interactions with the ligands is large compared with kT at room temperature. Magnetic measurements on the paramagnetic complexes **2**−**7** are consistent with the large splitting of the f orbitals observed in the NIR spectra. Specifically, only a single occupied state is observed to relatively high temperature in most of these complexes, and the values of μ_{eff} at 300 K are considerably smaller than that of the free ion. Most remarkable in this series of bis(μ-oxo) diuranium complexes is the observation that the U^V/U^V dimer **3** displays unusually strong antiferromagnetic coupling with T_N = 70 K.

The magnetic susceptibility was fit using the magnetic susceptibility of the U^V center in **7** to model the magnetic susceptibility of a magnetically isolated U^V center with the same crystal field as **3**. The resulting effective spin coupling constants are $\hat{J}_{\parallel} = -65\ cm^{-1}$ and $\hat{J}_{\perp} = -10\ cm^{-1}$. The value of $\hat{J}_{\parallel}$ is the largest reported for a U^V complex, and while a larger value of T_N has been observed in a U^{III} inverse sandwich complex, fitting the magnetic susceptibility of that complex to determine the coupling constant has not been possible.

■ ASSOCIATED CONTENT

Ⓢ Supporting Information

Supporting graphics, experimental conditions, synthetic procedures, and spectroscopic data. This material is available free of charge via the Internet at http://pubs.acs.org.

■ AUTHOR INFORMATION

Corresponding Authors

wwlukens@lbl.gov

karsten.meyer@fau.de

Notes

The authors declare no competing financial interest.

■ ACKNOWLEDGMENTS

Dedicated to the memory of Dr. Lester R. Morss for his friendship and encouragement. Support from the Bundesministerium für Bildung and Forschung (BMBF 2020+, 02NUK012B), the FAU Erlangen-Nürnberg, and COST Action CM1006 is acknowledged. Portions of this work were supported by the U.S. Department of Energy, Office of Basic Energy Sciences, Chemical Sciences, Biosciences, and Geosciences Division, Heavy Element Chemistry Program and were performed at Lawrence Berkeley National Laboratory under Contract DE-AC02-05CH11231. We thank Dr. A. K. Abdul-Sada and Prof. F. Geoffrey N. Cloke for performing mass spectrometry experiments. Furthermore, we gratefully acknowledge Prof. Dr. Dirk M. Guldi for use of his Raman spectrometer and Dipl. Chem. Tobias Engesser and Prof. Dr. Ingo Krossing for kindly providing $Ag[Al(OC(CF_3)_3)_4]$ and $NO[Al(OC(CF_3)_3)_4]$.

■ REFERENCES

(1) Zhang, Z.; Pitzer, R. M. *J. Phys. Chem. A* **1999**, *103*, 6880−6886.

(2) (a) Burns, C. J.; Eisen, M. S. In *The Chemistry of the Actinide and Transactinide Elements*, 3rd ed.; Morss, L. R., Edelstein, N. M., Fuger, J., Eds.; Springer: Dordrecht, The Netherlands, 2006; Vol. *5*, Chapter 25. (b) Zalkin, A.; Beshouri, S. M. *Acta Crystallogr., Sect. C* **1988**, *10*, 1826−1827. (c) Zi, G.; Jia, L.; Werkema, E. L.; Walter, M. D.; Gottfriedsen, J. P.; Andersen, R. A. *Organometallics* **2005**, *24*, 4251−4264. (d) Arney, D. S. J.; Burns, C. J. *J. Am. Chem. Soc.* **1993**, *115*, 9840−9841. (e) Fortier, S.; Kaltsoyannis, N.; Wu, G.; Hayton, T. W. *J. Am. Chem. Soc.* **2011**, *133*, 14224−14227. (f) Fortier, S.; Brown, J. L.; Kaltsoyannis, N.; Wu, G.; Hayton, T. W. *Inorg. Chem.* **2012**, *51*, 1625−1633. (g) Lam, O. P.; Heinemann, F. W.; Meyer, K. *Chem. Sci.* **2011**, *2*, 1538−1547. (h) Arney, D. S. J.; Burns, C. J. *J. Am. Chem. Soc.* **1995**, *117*, 9448−9460. (i) de Wet, J. F.; du Preez, J. G. H. *J. Chem. Soc., Dalton Trans.* **1978**, 592−597. (j) Kosog, B.; La Pierre, H. S.; Heinemann, F. W.; Liddle, S. T.; Meyer, K. *J. Am. Chem. Soc.* **2012**, *134*, 5284−5289. (k) Mills, D. P.; Cooper, O. J.; Tuna, F.; McInnes, E. J. L.; Davies, E. S.; McMaster, J.; Moro, F.; Lewis, W.; Blake, A. J.; Liddle, S. T. *J. Am. Chem. Soc.* **2012**, *134*, 10047−10054. (l) Lewis, A. J.; Carroll, P. J.; Schelter, E. J. *J. Am. Chem. Soc.* **2013**, *135*, 13185−13192. (m) Lewis, A. J.; Carroll, P. J.; Schelter, E. J. *J. Am. Chem. Soc.* **2012**, *134*, 511−518. (n) Cooper, O.; Camp, C.; Pécaut, J.; Kefalidis, C. E.; Maron, L.; Gambarelli, S.; Mazzanti, M. *J. Am. Chem. Soc.* **2014**, *136*, 6716−6723.

(3) Jones, G. M.; Arnold, P. L.; Love, J. B. *Angew. Chem., Int. Ed.* **2012**, *51*, 12584−12587.

(4) Labouille, S.; Clavaguéra, C.; Nief, F. *Organometallics* **2013**, *32*, 1265−1271.

(5) (a) Lukens, W. W.; Edelstein, N. M.; Magnani, N.; Hayton, T. W.; Fortier, S.; Seaman, L. A. *J. Am. Chem. Soc.* **2013**, *135*, 10742−10754. (b) Roger, M.; Belkhiri, L.; Arliguie, T.; Thuery, P.; Boucekkine, A.; Ephritikhine, M. *Organometallics* **2008**, *27*, 33−42. (c) Camp, C.; Antunes, M. A.; García, G.; Ciofini, I.; Santos, I. C.; Pécaut, J.; Almeida, M.; Marçalo, J.; Mazzanti, M. *Chem. Sci.* **2014**, *5*, 841−846. (d) Minasian, S. G.; Krinsky, J. L.; Arnold, J. *Chem.—Eur. J.* **2011**, *17*, 12234−12245. (e) Kaltsoyannis, N. *Inorg. Chem.* **2012**, *51*, 3407−3413. (f) Neidig, M. L.; Clark, D. L.; Martin, R. L. *Coord. Chem. Rev.* **2013**, *257*, 394−406.

(6) (a) Chatelain, L.; Mougel, V.; Pécaut, J.; Mazzanti, M. *Chem. Sci.* **2012**, *3*, 1075−1079. (b) Mougel, V.; Horeglad, P.; Nocton, G.; Pécaut, J.; Mazzanti, M. *Angew. Chem., Int. Ed.* **2009**, *48*, 8477−8480. (c) Nocton, G.; Horeglad, P.; Pécaut, J.; Mazzanti, M. *J. Am. Chem. Soc.* **2008**, *130*, 16633−16645. (d) Spencer, L. P.; Schelter, E. J.; Yang, P.; Gdula, R. L.; Scott, B. L.; Thompson, J. D.; Kiplinger, J. L.; Batista, E. R.; Boncella, J. M. *Angew. Chem., Int. Ed.* **2009**, *48*, 3795−3798. (e) Rosen, R. K.; Andersen, R. A.; Edelstein, N. M. *J. Am. Chem. Soc.* **1990**, *112*, 4588−4590. (f) Arnold, P. L.; Jones, G. M.; Odoh, S. O.; Schreckenbach, G.; Magnani, N.; Love, J. B. *Nat. Chem.* **2012**, *4*, 221−227. (g) Korobkov, I.; Gambarotta, S.; Yap, G. P. A. *Angew. Chem., Int. Ed.* **2002**, *41*, 3433−3436. (h) Rinehart, J. D.; Harris, T. D.; Kozimor, S. A.; Bartlett, B. M.; Long, J. R. *Inorg. Chem.* **2009**, *48*, 3382−3395. (i) Diaconescu, P. L.; Arnold, P. L.; Baker, T. A.; Mindiola, D. J.; Cummins, C. C. *J. Am. Chem. Soc.* **2000**, *122*, 6108−6109.

(7) Umetsu, R. Y.; Okamoto, Y.; Miyakawa, M.; Sasao, K.; Fukamichi, K.; Sakuma, A. *J. Magn. Magn. Mater.* **2004**, *272−276*, 790−791.
(8) Figgis, B. N.; Martin, R. L. *J. Am. Chem. Soc.* **1956**, *78*, 3837−3846.
(9) Vlaisavljevich, B.; Diaconescu, P. L.; Lukens, W. L.; Gagliardi, L.; Cummins, C. C. *Organometallics* **2013**, *32*, 1341−1352.
(10) Schmidt, A.-C.; Nizovtsev, A. V.; Scheurer, A.; Heinemann, F. W.; Meyer, K. *Chem. Commun.* **2012**, *48*, 8634−8636.
(11) Brown, J. L.; Fortier, S.; Lewis, R. A.; Wu, G.; Hayton, T. W. *J. Am. Chem. Soc.* **2012**, *134*, 15468−15475.
(12) (a) Hazra, S.; Majumder, S.; Fleck, M.; Mohanta, S. *Polyhedron* **2008**, *27*, 1408−1414. (b) Duval, P. B.; Burns, C. J.; Buschmann, W. E.; Clark, D. L.; Morris, D. E.; Scott, B. L. *Inorg. Chem.* **2001**, *40*, 5491−5496. (c) Spencer, L. P.; Yang, P.; Scott, B. L.; Batista, E. R.; Boncella, J. M. *Inorg. Chem.* **2009**, *48*, 11615−11623. (d) Wahu, S.; Berthet, J.-C.; Thuéry, P.; Guillaumont, D.; Ephritikhine, M.; Guillot, R.; Cote, G.; Bresson, C. *Eur. J. Inorg. Chem.* **2012**, 3747−3763.
(13) Bart, S. C.; Anthon, C.; Heinemann, F. W.; Bill, E.; Edelstein, N. M.; Meyer, K. *J. Am. Chem. Soc.* **2008**, *130*, 12536−12546.
(14) Multiple attempts to remove the two μ-oxo-bound K^+ ions in **6** by encapsulation with a crown ether or cryptand led to an entirely new product. A single new species was isolated in moderate yield from the reaction of **6** with 2.2.2-cryptand. This new product, as confirmed by ^{1}H NMR spectroscopy and a single-crystal X-ray diffraction study (see the Supporting Information), was identified as [K(2.2.2-crypt)][{((^{nP,Me}ArO)$_3$tacn)U$^{IV/IV}$}$_2$(μ-O)(μ-OH)] (**10**). Closer inspection of the molecular structure of **10** revealed the loss of the typical U(μ-O)$_2$U diamond core structural motif. Instead, complex **10** exhibits a U^{IV}(μ-O)(μ-OH)U^{IV} core structure with two shorter U−μ-O bonds at 2.120(3)/2.163(3) Å and two longer U−μ-OH bonds at 2.282(3)/2.267(3) Å. This reaction supports the assumption that the two μ-oxo-bound K^+ are crucial for the stabilization of the U(μ-O)$_2$U diamond core in **6**.
(15) Lam, O. P.; Heinemann, F. W.; Meyer, K. *C. R. Chim.* **2010**, *13*, 803−811.
(16) La Pierre, H. S.; Meyer, K. *Inorg. Chem.* **2013**, *51*, 529−539.
(17) Castro-Rodriguez, I.; Olsen, K.; Gantzel, P.; Meyer, K. *Chem. Commun.* **2002**, 2764−2765.
(18) Graves, C. R.; Yang, P.; Kozimor, S. A.; Vaughn, A. E.; Clark, D. L.; Conradson, S. D.; Schelter, E. J.; Scott, B. L.; Thompson, J. D.; Hay, P. J.; Morris, D. E.; Kiplinger, J. L. *J. Am. Chem. Soc.* **2008**, *130*, 5272−5285.
(19) (a) Richardson, D. E.; Taube, H. *Inorg. Chem.* **1981**, *20*, 1278−1285. (b) Fox, A. R.; Arnold, P. L.; Cummins, C. C. *J. Am. Chem. Soc.* **2010**, *132*, 3250−3251.
(20) Guokui, L.; Beitz, J. V. In *The Chemistry of the Actinide and Transactinide Elements*, 3rd ed.; Morss, L. R., Edelstein, N. M., Fuger, J., Eds.; Springer: Dordrecht, The Netherlands, 2006; Vol. *3*, Chapter 18.
(21) (a) Mizuoka, K.; Tsushima, S.; Hasegawa, M.; Hoshi, T.; Ikeda, Y. *Inorg. Chem.* **2005**, *44*, 6211−6218. (b) Nocton, G.; Horeglad, P.; Vetere, V.; Pécaut, J.; Dubois, L.; Maldivi, P.; Edelstein, N. M.; Mazzanti, M. *J. Am. Chem. Soc.* **2009**, *131*, 495−508.
(22) Ryan, J. L. *J. Inorg. Nucl. Chem.* **1971**, *33*, 153−177.
(23) Selbin, J.; Sherrill, H. J. *Inorg. Chem.* **1974**, *113*, 1235−1239.
(24) Fortier, S.; Wu, G.; Hayton, T. W. *Inorg. Chem.* **2008**, *47*, 4752−4761.
(25) Graves, C. R.; Vaughn, A. E.; Schelter, E. J.; Scott, B. L.; Thompson, J. D.; Morris, D. E.; Kiplinger, J. L. *Inorg. Chem.* **2008**, *47*, 11879−11891.
(26) Thomson, R. K.; Scott, B. L.; Morris, D. E.; Kiplinger, J. L. *C. R. Chim.* **2010**, *13*, 790−802.
(27) Lever, A. B. P. *Inorganic Electronic Spectroscopy*; Elsevier Applied Science: Amsterdam, 1984; Vol. *2*.
(28) Kraft, S. J.; Williams, U. J.; Daly, S. R.; Schelter, E. J.; Kozimor, S. A.; Boland, K. S.; Kikkawa, J. M.; Forrest, W. P.; Christensen, C. N.; Schwarz, D. E.; Fanwick, P. E.; Clark, D. L.; Conradson, S. D.; Bart, S. C. *Inorg. Chem.* **2011**, *50*, 9838−9848.
(29) (a) Cooper, S. R.; Calvin, M. *J. Am. Chem. Soc.* **1977**, *99*, 6623−6630. (b) Larsen, P. L.; Parolin, T. J.; Powell, D. R.; Hendrich, M. P.; Borovik, A. S. *Angew. Chem., Int. Ed.* **2003**, *42*, 85−89. (c) Galas, A. M. R.; Hursthouse, M.; Behrman, E. J.; Midden, W. R.; Green, G.; Griffith, W. P. *Transition Met. Chem.* **1981**, *6*, 194−195.
(30) (a) Aboelella, N. W.; Lewis, E. A.; Reynolds, A. M.; Brennessel, W. W.; Cramer, C. J.; Tolman, W. B. *J. Am. Chem. Soc.* **2002**, *124*, 10660−10661. (b) Mahapatra, S.; Halfen, J. A.; Wilkinson, E. C.; Pan, G.; Wang, X.; Young, V. G., Jr.; Cramer, C. J.; Que, L., Jr.; Tolman, W. B. *J. Am. Chem. Soc.* **1996**, *118*, 11555−11574.
(31) (a) Dong, Y.; Fujii, H.; Hendrich, M. P.; Leising, R. A.; Pan, G.; Randall, C. R.; Wilkinson, E. C.; Zang, Y.; Que, L., Jr. *J. Am. Chem. Soc.* **1995**, *117*, 2778−2792. (b) Gamelin, D. R.; Kirk, M. L.; Stemmler, T. L.; Pal, S.; Armstrong, W. H.; Penner-Hahn, J. E.; Solomon, E. I. *J. Am. Chem. Soc.* **1994**, *116*, 2392−2399. (c) Schenker, R.; Mandimutsira, B. S.; Riordan, C. G.; Brunold, T. C. *J. Am. Chem. Soc.* **2002**, *124*, 13842−13855.
(32) (a) King, D. M.; Tuna, F.; McMaster, J.; Lewis, W.; Blake, A. J.; McInnes, E. J. L.; Liddle, S. T. *Angew. Chem., Int. Ed.* **2013**, *52*, 4921−4924. (b) Lewis, A. J.; Nakamaru-Ogiso, E.; Kikkawa, J. M.; Carroll, P. J.; Schelter, E. J. *Chem. Commun.* **2012**, *48*, 4977−4979.
(33) Kahn, O. *Angew. Chem., Int. Ed. Engl.* **1985**, *24*, 834−850.
(34) (a) Van Vleck, J. H. *The Theory of Electric and Magnetic Susceptibilities*; Clarendon Press: Oxford, U.K., 1932. (b) Gerloch, M. *Magnetism and Ligand-Field Analysis*; Cambridge University Press: Cambridge, U.K., 1983.
(35) Stevens, K. W. H. *Proc. R. Soc. London, Ser. A* **1953**, *219*, 542−555.
(36) Zuend, S. J.; Lam, O. P.; Heinemann, F. W.; Meyer, K. *Angew. Chem.* **2011**, *123*, 10814−10818.
(37) Siladke, N. A.; Meihaus, K. R.; Ziller, J. W.; Fang, M.; Furche, F.; Long, J. R.; Evans, W. J. *J. Am. Chem. Soc.* **2012**, *134*, 1243−1249.
(38) Lane, B. C.; Venanzi, L. M. *Inorg. Chim. Acta* **1969**, *3*, 239−245.
(39) Flint, C. D.; Tanner, P. A. *Mol. Phys.* **1987**, *61*, 389−407.
(40) Carretta, S.; Amoretti, G.; Santini, P.; Mougel, V.; Mazzanti, M.; Gambarelli, S.; Colineau, E.; Caciuffo, R. *J. Phys.: Condens. Matter* **2013**, *25*, No. 486001.
(41) Lukens, W. W.; Walter, M. D. *Inorg. Chem.* **2010**, *49*, 4458−4465.
(42) Costes, J.-P.; Dahan, F.; Dupuis, A.; Laurent, J.-P. *Chem.—Eur. J.* **1998**, *4*, 1616−1620.
(43) Abragam, A.; Bleaney, B. *Electron Paramagnetic Resonance of Transition Ions*; Clarendon Press: Oxford, U.K., 1970.
(44) Jones, E. R., Jr.; Hendricks, M. E.; Stone, J. A.; Karraker, D. G. *J. Chem. Phys.* **1974**, *60*, 2088−2094.
(45) (a) Jones, W. M.; Gordon, J.; Long, E. A. *J. Chem. Phys.* **1952**, *20*, 695−699. (b) Vogt, O.; Mattenberger, K.; Löhle, J. *J. Magn. Magn. Mater.* **2001**, *231*, 199−212.